Applied Physics Reviews

REVIEW ARTICLE | APRIL 21 2025

Recent advances in fluidic neuromorphic computing

Cheryl Suwen Law ; Juan Wang ; Kornelius Nielsch ; Andrew D. Abell ; Juan Bisquert ;
Abel Santos

Appl. Phys. Rev. 12, 021309 (2025)
https://doi.org/10.1063/5.0235267

Applied Physics Reviews REVIEW pubs.aip.org/aip/are

Recent advances in fluidic neuromorphic computing

Cite as: Appl. Phys. Rev. 12, 021309 (2025); doi: 10.1063/5.0235267
Submitted: 26 August 2024 · Accepted: 1 April 2025 ·
Published Online: 21 April 2025

View Online Export Citation CrossMark

Cheryl Suwen Law,[1,2,a)] Juan Wang,[1,2] Kornelius Nielsch,[3] Andrew D. Abell,[2,4] Juan Bisquert,[5,a)] and Abel Santos[1,2,a)]

AFFILIATIONS

[1]School of Chemical Engineering, The University of Adelaide, Adelaide, South Australia 5005, Australia
[2]Institute for Photonics and Advanced Sensing, The University of Adelaide, Adelaide, South Australia 5005, Australia
[3]Leibniz Institute for Solid State and Materials Research (IFW), 01069 Dresden, Germany
[4]Department of Chemistry, The University of Adelaide, Adelaide, South Australia 5005, Australia
[5]Instituto de Tecnología Química (Universitat Politècnica de València-Agencia Estatal Consejo Superior de Investigaciones Científicas), Av. dels Tarongers, 46022 València, Spain

[a)]**Authors to whom correspondence should be addressed:** cherylsuwen.law@adelaide.edu.au; jbisquer@itq.upv.es; and abel.santos@adelaide.edu.au

ABSTRACT

Human brain is capable of optimizing information flow and processing without energy-intensive data shuttling between processor and memory. At the core of this unique capability are billions of neurons connected through trillions of synapses—basic processing units of the brain. The action potentials or "spikes" based temporal processing using the regulated flow of ions across ion channels in neuron cells allows sparse and efficient transmission of data in the brain. Emerging systems based on confined fluidic systems have provided a framework for a new type of neuromorphic computing with lower energy consumption, hardware-level plasticity, and multiple information carriers that emulate natural processes and mechanisms of human brain. These systems mimic neuronal architectures by harnessing and modulating ion transport along artificial channels. The spikes-induced ion-to-surface interactions within these fluidic systems enables the control of ionic conductivity to achieve synaptic plasticity for the realization of brain-inspired functionalities such as memory effect and signal transmission. Herein, this review provides an overview of recent advances in fluidic devices such as memristors and other computing components, covering their basic operations, materials and architectures, as well as applications in neuromorphic computing. The review concludes with a brief outline of the challenges that these emerging technologies face and an outlook for the development of fluidic-based brain-inspired computing.

TABLE OF CONTENTS

I. INTRODUCTION

Artificial intelligence (AI) technologies have seamlessly integrated into everyday life, from personalized content recommendations on streaming platforms to virtual assistants and facile recognition on smart devices.[1] The use of brain-inspired algorithms such as artificial neural networks have demonstrated exceptional success in machine learning, having a transformative impact across various sectors such as medical diagnosis, security, robotics, and the Internet of Things.[2–4] It is undeniable that AI will reshape the future of manufacturing, healthcare, navigation, and transportation. However, these advances will require critical advances in the performance of current electronic devices—to meet the exponentially growing demand of computation capability to perform data-driven decision-making tasks.[4]

Although machine learning algorithms based on neural networks offer a more energy efficient approach to process information in a distributed and adaptive fashion, they are typically realized using conventional von Neumann computing architectures, which suffer from processing limitations and excessive power consumption.[4,5] To overcome the von Neumann bottleneck, new devices and computing principles have been devised for circumventing the intrinsic constraints of conventional computing technology and the physical limits of Moore's law.[6] Of all these, the emergence of neuromorphic computing inspired by the brain's architecture—a biological circuit composed of neurons interconnected by synapses that implement memory *in situ* and in a nonvolatile manner—has shown promising results to address the shortcomings of conventional computation.[7] In the brain, information processing occurs inside neuron somas via analog computation, whereas neurons communicate with each other via binary voltage spikes.[7] By emulating neurons and synapses, neuromorphic engineering aims to gaining speed and energy efficiency to performing complex computation tasks through massively distributed and parallel memory and computation elements.[8] Current neuromorphic computing mostly uses conventional electronic materials, in particular, silicon-based complementary metal–oxide–semiconductor (CMOS) spiking neural networks. The practical applicability of these systems has been demonstrated by IBM's NorthPole and TrueNorth chips, SynSense's XYLO^{TM} and SPECK^{TM}, and Intel Corporation's Hala Point.[9–15] Despite these outstanding achievements, the potential of neuromorphic electronics based on CMOS technology to truly mimic the capability of the brain is limited due to its scalability, fan-out issues, and two–dimensional interconnectivity.[7] This has prompted the expansion of neuromorphic computing into the field of photonics and nanofluidics.[16–18] Photonics or optoelectronic neuromorphic systems have specific advantages such as wide bandwidth, increased data transport, and excellent interconnect with negligible resistor-capacitor delay and power loss. However, they require complicated wavelength conversion, sophisticated laser systems, and high optical power for all-optical nonlinear transfer functions, suggesting a complex and costly fabrication process.[19] Unlike optoelectronic and electronic computing, which use photons and electrons–holes as information carriers, respectively, fluidic-based neuromorphic computing harnesses ions in electrolyte solutions to imitate the brain's operating mechanism. Inspired by the parallel transport of various ionic and molecular species in aqueous environment in the brain's synapses, as depicted in Fig. 1(a), the control of ionic flow across biomimicking nanopores makes it possible to realize brain functionalities, i.e., synaptic plasticity and chemical regulation.[18,20] The benefits of using ions as transporters in neuromorphic computing are fourfold: (i) abundant chemical information in ionic currents due to the coexisting of a wide variety of freely moving ions; (ii) versatile chemical properties that make it possible to tailor specific chemical interactions similar to that of ligand–gated ion channels in neurons; (iii) connection between hardware and neurons via both electrical and chemical communications; and (iv) robustness to electrical and magnetic interferences.[21,22] The unique characteristics of ions offer the possibility of producing highly parallel computing devices with complex neuromorphic functions whereas requiring less circuit complexity and energy consumption using a fluidic approach. The transport phenomena of charged ionic species across fluidic systems as a result of interfacial interactions and spatial confinement enables these bioinspired architectures to operate as synthetic neurosynaptic devices.[23,24] These ion-controlled systems are usually in the form of micrometer and nanometer sized channels and pores composed of silica, anodic alumina, polymers, and glass, where their structural and chemical properties can be engineered for the precise modulation of ionic flow and the concomitant current signals.[25] This unique approach enables unique transport behaviors associated with ion concentration polarization,[26] ion adsorption on channel walls,[27] movement of liquid–liquid interface,[28] variation in ion aggregation states,[29] and switching of ion channels.[30] These differential advantages make fluidic systems a powerful approach to realize true synaptic plasticity through distinct ionic conducting properties.[31] Therefore, they can behave as memristors with memory effect, or iontronic components with the ability of ion gating such as diodes that rectify ionic flow, for the development of fluidic neuromorphic systems based on layered neural networks or reservoir computing [Fig. 1(b)].[32]

In this context, this review compiles the recent advances on fluidic-based memristors and other iontronic components, focusing on three main aspects: (i) fundamental operations; (ii) materials and architectures; and (iii) recent advances in neuromorphic computing

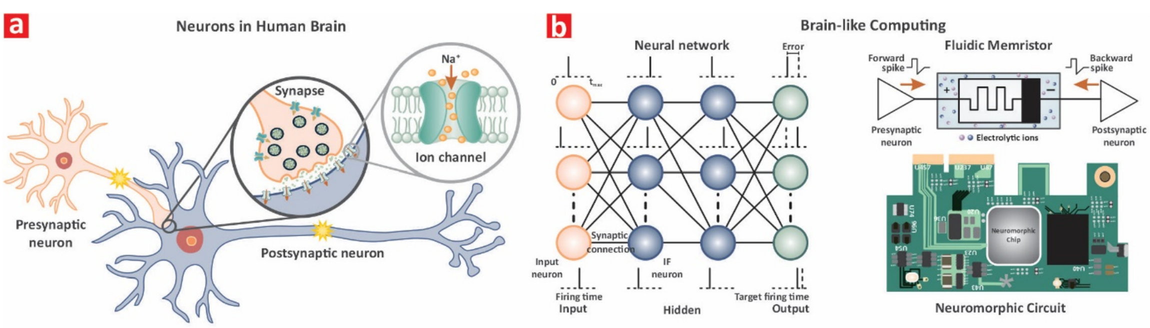

FIG. 1. Neuromorphic computing inspired by biological neural systems. (a) Illustration of the generation and transmission of signals using ions in synapses and ion channels in the brain. (b) Bioinspired ion-based computing based on neural network using fluidic memristors and other fluidic components.

with representative examples. This review concludes with a general overview and a prospective outlook on the future development of brain-inspired fluidic-based computing.

II. FLUIDIC MEMRISTORS

A. Fundamental principles

Inspired by the human brain functions such as processing and memory units based on analog signals, analog in-memory computing can be realized by memristors—resistive systems with inherent memory.[33] A memristor is basically a two terminal structure constituting two electrodes that deliver and receive electrical signals with a storage layer in between, as described in Fig. 2(a). The dynamic reconfiguration of the storage layer in response to electrical stimulation, as illustrated in Fig. 2(b), results in memory effects, in which the internal resistance state can be retained according to the history of applied voltage (V_{app}) and current.[6,34] A memristor is capable of mimicking synaptic and neural functions while integrating memory and logic operations in a single unit.[35] Fluidic memristive systems have been developed by adapting the working mechanism of synapses, which use ions moving in fluids to carry and store information in detection of chemical and electrical signals.[20,21] Analogous to the transport of neurotransmitters in synapses triggered by spike-form synaptic events that induce a change in synaptic weight, spike-form electrical pulses cause an alteration of the conductivity of the memristor due to the variation in the directional movement of ions in its fluidic matrix.[36]

The history-dependent properties of a fluidic memristor are associated with the differences in the kinetics between the applied potential sweep and its corresponding ion transport behavior.[37,38] The ion transport of a fluidic memristor is characterized by its I–V curve, which features a hysteresis loop that is pinched at a cross-point potential under a bipolar voltage sweep, as depicted in Fig. 2(c).[32,39] The cross-point potential denotes the transition between high and low conductivity states, where there is a balance between bias potential and average surface potential.[26,39] The current amplitude under a forward potential scan from low to high conduction states is lower than that of backward scan from high to low conduction states.[26] Under biases that are more negative than the cross-point potential, the hysteresis that occurs at low conduction state corresponds to a normal capacitive behavior and a positive phase shift of current. The hysteresis at high conduction state shows a negative phase shift of current responses in correlation to the applied scanning potential waveform, hence revealing a negative capacitance or an inductive behavior.[37] The difference between forward and backward current reflects ion transport hysteresis and its residual charges quantification based on the integration of change in current over a time duration determines the hysteresis ionic enrichment and depletion dynamics.[26,40] Generally, the hysteresis effects in nanopores can be described by the Hodgkin and Huxley (HH)-inspired model, which consists of the following equations:

$$I_{\mathrm{tot}}(u) = [g_L + (g_H - g_L)x](u - E_o), \tag{1}$$

$$\tau_k(u)\frac{dx}{dt} = x_{\mathrm{eq}}(u) - x, \tag{2}$$

where I_{tot} is the current across the nanopore, g_H and g_L are conductances at high and low values, respectively, u is voltage, x is fractional occupancy of a conducting state for channel conductance activation, (u–E_0) is the driving force for current, τ_k is the relaxation time of activation, and x_{eq} is activation variable at equilibrium.[41] These equations can be further developed for various scenarios, i.e., different architecture and operation of memristors, and they have been extensively reviewed and discussed elsewhere.[24,29,42,43] It is worthwhile to note that some fluidic memristors exhibit negative differential resistance effect (NDR)—an inverse correlation between current and voltage, which is a functional part of spiking neurons.[41,44,45] Some also show resistive switching characteristic that involves a voltage-driven change in the resistance state between high and low values for the implementation of basic synaptic functions.[41,46]

B. Memristive artificial synapse functionality and mechanism

A standard biological synapse comprises a pre-synaptic neuron and a post-synaptic neuron linked by a synaptic cleft. In a memristor-based artificial synapse, the bottom and top contacts function as neurons, while the switchable conducting layer, e.g., the nanopore channel, serves as synaptic connection.[47] The device's electrical conductivity represents the synaptic weight, and the plasticity of the synapse indicates how the conductivity is influenced by the interconnected neurons. A widely studied plasticity mechanism is spike-time dependent plasticity (STDP) that modifies the synaptic weight according to the relative timing of spikes between pre- and post-synaptic neurons. Several bio-inspired synaptic functions can be developed, and some examples are short-term and Hebbian plasticity, meta-plasticity

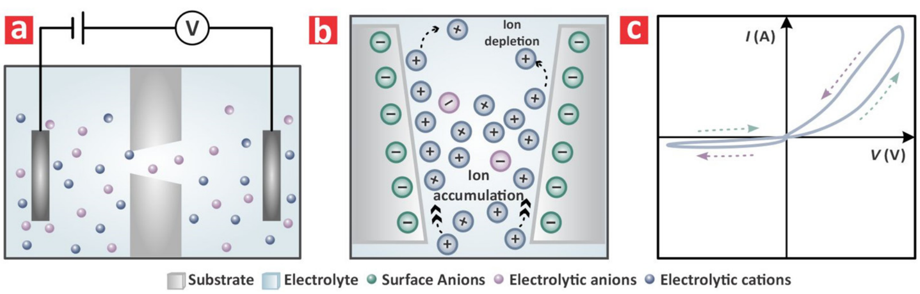

FIG. 2. Fundamental principles of fluidic memristors. (a) A representative setup of a fluidic memristor consisting of a nanochannel and two Ag/AgCl electrodes immersed in electrolyte solution. (b) Illustration of kinetic-dependent ion depletion and accumulation within the nanochannel (single- and triple-headed arrows indicate slow and fast rate, respectively). (c) Current–voltage (I–V) profile of fluidic memristor characterized by pinched hysteresis loops with green and purple arrows indicate forward and backward sweep, respectively.

(control of neural state over the decay time),[48] time-dependent (pair and triplet STDP), and rate-dependent (Bienenstock–Cooper–Munro) synaptic learning rules.[49] Here, we provide some insights to the operation of fluidic nanochannels in the increase or decrease in the ionic conductivity in response to applied voltage spikes, that corresponds to potentiation or depression, respectively, of the memristive synapse.

The characterization of fluidic pores using cyclic voltammetry at different frequencies unveils the ionic conduction, rectification, and hysteresis properties that lie behind the synapse operation.[41] Figure 3(a-i) shows a typical behavior of a representative nanopore-based fluidic memristor system theoretically modeled using Eqs. (1) and (2).[50] At high scan rate, the fast current [green line in Fig. 3(a-i)] remains at low conductance level in both $V_{app} < 0$ and $V_{app} > 0$. At low scan rate, the output current progressively reaches a high conductance level at $V_{app} > 0$ [red line in Fig. 3(a-i)], which eventually reaches a stationary current [gray line in Fig. 3(a-i)]. The asymmetric current–voltage (I–V) response is attributed to rectification effect, where high current is suppressed when $V_{app} < 0$. At intermediate scan frequency one obtains the inductive loops (counterclockwise) at the positive side. Since the current is self-crossing the current becomes capacitive (clockwise) at the negative side. These denominations, i.e., inductive and capacitive, correspond to the general behavior of a conducting system with hysteresis.[38,51] They can be correlated with the dominant behavior observed in the impedance spectra at separate voltage domains.[52] The properties of alternating current impedance analysis are indicated by the equivalent circuits shown in Fig. 3(a-ii) that can be calculated from Eqs. (1) and (2).[41] The inductive behavior is obtained by the chemical inductor feature that is caused by Eq. (2).[53] This is due to the delay polarization

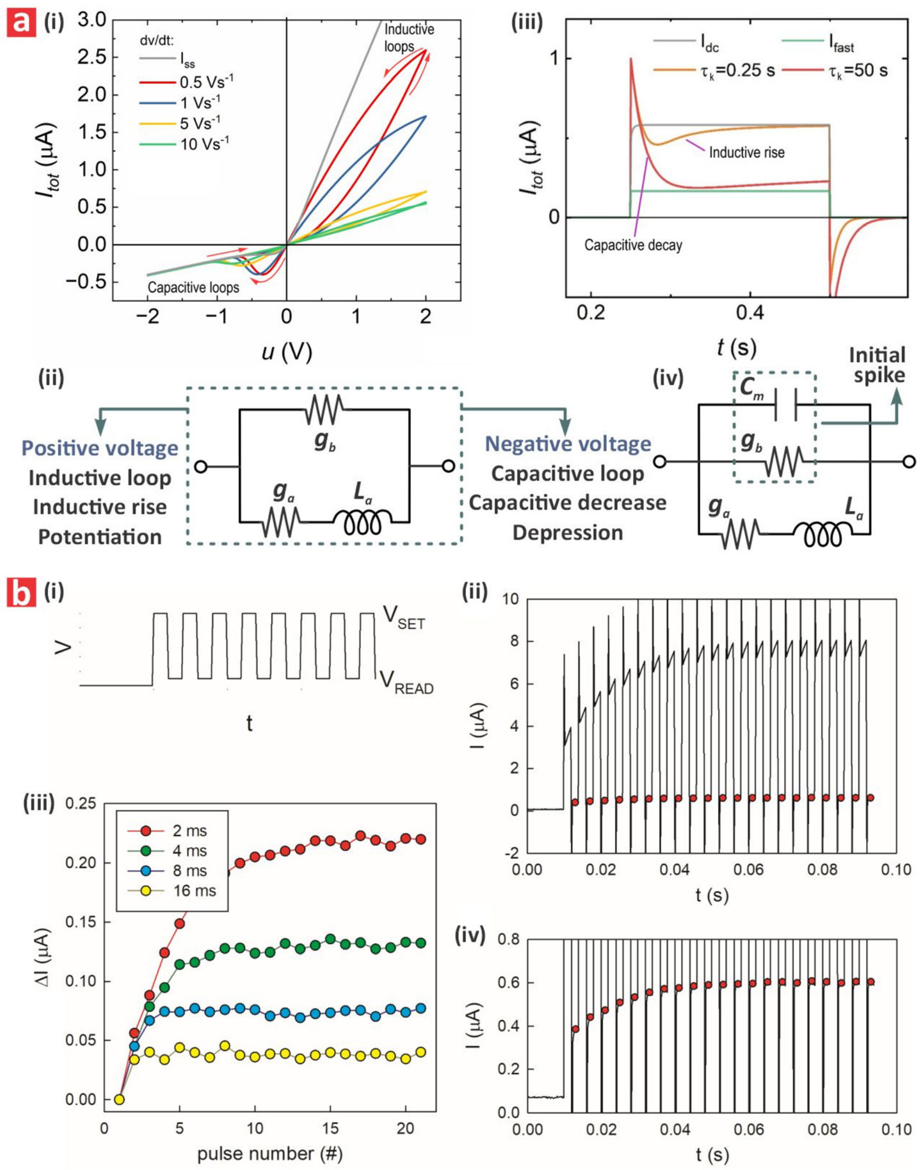

FIG. 3. Operations of nanoporous membranes as a representative fluidic memristor in correlation to potentiation and depression of synapse. (a) Theoretical models of synaptic behavior in a nanopore: (i) current cycling response at different scan rates simulated based on Eqs. (1) and (2); (ii) small signal equivalent circuit interpretation of the dynamical regimes in (i); (iii) model current response to a voltage step pulse comprising slow and fast components of the current, and transient current under two different characteristic relaxation time (τ_k); and (iv) equivalent circuit with the incorporation of a constant capacitor. Reprinted (adapted) with permission from Bisquert *et al.*, Phys. Chem. Chem. Phys. **26**, 13804–13813 (2024). Copyright 2024 Authors; licensed under a Creative Commons Attribution (CC BY) license.[50] (b) Experimental synaptical response of nanoporous polymer membranes based on the average reading current increase in response to a train of voltage pulses with various reading times between SET voltage steps with a READ voltage of 0.1 V: (i) schematic of voltage train pulses to stimulate fluidic nanopores; (ii) the complete current response to a train of 20 voltage pulses of 2 ms separated by 2 ms reading steps; (iii) the change in current response as a function of reading time; and (iv) a magnified view of the current response at the scale of reading voltage. Reprinted (adapted) with permission from Bisquert *et al.*, ChemPhysChem **25**, e202400265 (2024). Copyright 2024 Authors; licensed under a Creative Commons Attribution (CC BY) license.[54]

effect that affects the ionic conduction. Importantly, the same model generates a capacitive behavior at negative voltages.[50] This nontrivial result is obtained because the inductor and conductance g_a in Fig. 3(a-ii), both become negative.

Now we turn to the time domain features of the same model that govern the dominant adaptation properties of the synapse. They are shown in Fig. 3(a-iii) that displays the current response under a square voltage perturbation. The transient current usually shows an initial spike that decays with time. This is a typical response of charging a capacitive circuit. This capacitive behavior is obtained from an additional effect not included in Eqs. (1) and (2), the capacitive current charging the membrane (constant) capacitance (C_m), as shown in Fig. 3(a-iv). After the initial spike comes the active response of the ion conductance across the pore channel, that shows an inductive behavior as commented in Fig. 3(a-ii). Therefore, the current in Fig. 3(a-iii) raises with time, with a characteristic relaxation time (τ_k). If τ_k is short with respect to the perturbation time, the full slow current [gray line in Fig. 3(a-iii)] will be completed. However, if the relaxation time is long, the current will rise only a fraction of the possible value.

As shown in Fig. 3(b), that is obtained in representative experimental measurements, under a train of voltage pulses, the stepwise inductive raising current behavior causes the synaptical modulation.[54] Figure 3(b-i) indicates the change in voltage from a SET value that stimulates the synapse to a READ value that will be used in governing the computational signal.[55] In Fig. 3(b-iv), a clear increase in conductance associated with the positive voltage pulses, that forms the synapse potentiation, is demonstrated. Figure 3(b-iii) shows that the interval between pulses influences both the stimulation and the resulting change in conductivity, with an increased pulse frequency leading to greater stimulation. Consequently, the conductance of the device can be gradually adjusted by modifying the duration and sequence of the applied programming voltage, allowing it to reach different conductance states. Based on these insights, one can proceed to show other properties observed in biological synapses, such as the paired pulse facilitation (PPF) that consists of an enhancement in the amplitude of the second of two rapidly induced excitatory postsynaptic potentials.[56] It is also important to remark that τ_k can become a strong function of voltage, as occurs in Hodgkin–Huxley model.[50,57] The function of τ_k provokes an additional control of relaxation properties, such as metaplasticity, memristor volatility, and retention time.[48,58,59]

A broader set of results in synaptical stimulation of a nanopore membrane is presented in Fig. 4.[60] The I–V and current–time (I–t) curves at neutral pH [Figs. 4(a-i) and 4(b-i)] demonstrate the same potentiation effect at positive voltages already remarked in Fig. 3. However, in Fig. 4(b-i), another phenomenon is observed at negative voltage: the increase in conductance gained at positive voltages is progressively decreased by the negative voltage pulses. This is the depression feature due to the conduction capacitance effect mentioned earlier in Fig. 2(a-ii).[50] Note the initial current spikes that occurs at all voltages, in Fig. 4(b), that invert the value when the voltage is switched on and off. This is the result of the membrane capacitance indicated in Fig. 3(b). This ultrafast feature gives an arc in the high frequency part of the impedance spectra, while the conduction memory effect produces either an inductor or capacitor, depending on the voltage range.[50,52] It is interesting to compare the behavior displayed in Fig. 4(a-iii) and 4(b-iii), corresponding to pH = 2.0. Here the rectification side has been inverted with respect to Figs. 4(a-i) and 4(b-i) by the change of sign of the surface charge.[60] Hence, potentiation occurs when the applied potential is negative, as shown in Fig. 4(b-iii). These results attest to the extraordinary versatility of fluidic nanopores for

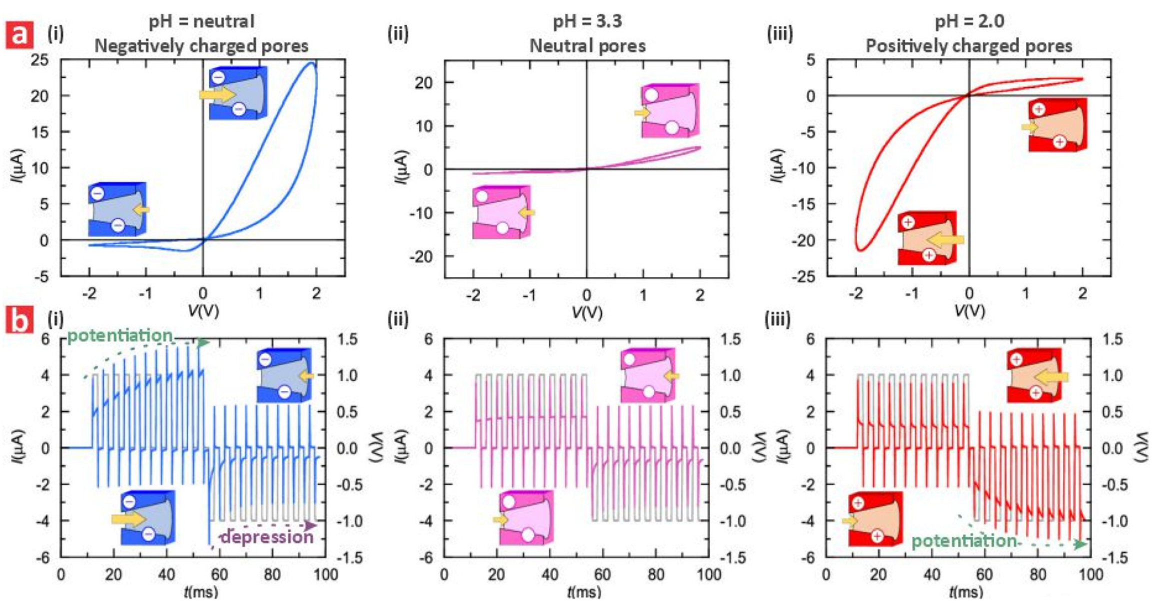

FIG. 4. Synaptical tunability of multipore nanofluidic membrane as a representative memristive system. (a) I–V profiles of nanoporous memristor showing pH-dependent ionic rectifying effect in 50 mM potassium chloride (KCl) solution at pH: (i) neutral, (ii) 3.3, and (iii) 2.0. (b) Current response to a sequence of positive voltage pulses of 2 ms with gradual conductance potentiation (indicated by green arrow) followed by a sequence of negative voltage pulses with a reset to low conductance state (depression indicated by purple arrow) at pH: (i) neutral, (ii) 3.3, and (iii) 2.0. Reprinted (adapted) with permission from Bisquert *et al.*, J. Phys. Chem. Lett. **14**, 10930–10934 (2023). Copyright 2023 American Chemical Society.[60]

neuromorphic circuits, since they can be modulated not just by electrical signals as ordinary memristors but also by chemical changes.[61,62]

C. Materials, architectures, and operations

Influenced by their working mechanism, fluidic memristors are developed in various channel or porous structures in one-, two-, and three-dimensions, using a variety of materials such as glass, polydimethylsiloxane (PDMS), graphite, MXene, and hydrogels.[23] The tuning of symmetricity, geometrical, and chemical properties of the artificial single or multiple channels are achieved by microfabrication and nanofabrication techniques, for instances: laser pulling, electron beam lithography and etching, photolithography, and reactive ion etching, in conjunction with chemical modifications.[23] The physics enabling voltage- and time-influenced conductivity and plasticity of fluidic memristors is established by the electrolyte behavior under spatial confinement, which involves electrolytic ion enrichment and depletion through polarization of the electric double layer (EDL), liquid–liquid interfacial interaction, formation of Bjerrum ion pairs, or surface adsorption/desorption of ions.[18,32,62] The ionic movement across the memristive system under an applied external bias polarizes the ion storage layer established by the surface electric field within the transport limiting region, leading to the redistribution of ions in this space.[62] The resulting surface effects from ion concentration polarization in the EDL further enrich ions in the high conductivity loop, while depleting ions in the low conductivity loop. As there is a delay between ion flux and scanned potential, i.e., ion flux does not return to zero at the instance bias is scanned to zero, the still-polarized EDL "remembers" the previous conductivity state and nonzero currents are detected. Therefore, this time-dependent ion concentration change contributes to the "memory effect."[37] The artificial channels used in this type of fluidic memristor are usually glass or polymeric nanocapillaries, nanopipettes, and nanopores with potassium chloride (KCl) as the electrolyte, as depicted in Fig. 5(a).[60,63,64] The surface chemistry of these artificial channels can also be tailored with charged molecules such as poly-L-lysine and Nafions to enhance the ion concentration polarization effect for memristive behavior.[65] One intriguing example is the modification of single nanopipette and anodic aluminum oxide membrane with PEDOT:PSS, where the reversible switching of PEDOT between positive and neutral form by oxidation and reduction modulates the space charge within the nanopore/membrane and induces hysteretic ion transport.[66]

The memristive effect that arises from liquid–liquid interfacial interactions is attributed to the ionic movement between two fluids of different conductance driven by electroosmotic flow.[61] Briefly, the electroosmotic flow effect is generated when the movement of the EDL in the direction of the applied electric field is transferred to the bulk liquid through viscous effect.[67,68] Due to the sluggish concentration polarization effect that comes along with the electroosmotic flow, the migration and local diffusion flux across the memristor shows a lag to the change in applied potential stimulus, with an enhancement of transport selectivity by electroosmotic flow. The variation in scanning potential also impacts the electrostatic screening and electroosmotic flow effect, and it causes a time-dependent change in conductance, as described by the pinched hysteretic current loops.[71–73] In this case, nanofluidic devices composed of PDMS with imprinted microchannels and nanochannels and sealed with a glass sheet, are used as interfacial memristors, as depicted in Fig. 5(b). The microchannels serve as reservoirs for two types of electrolytes with different conductance, i.e., ionic liquid and water, whereas the nanochannel is where the two reservoirs meet.[28,72] A micropore formed on silicon nitride substrate subjected to a salinity gradient can also function as an interfacial memristor.[46] Considering the electroosmotic flow effect in terms of fluid flow type (axial or spiral), tapered conical nanopore in KCl electrolyte have different ion concentrations at various positions along its axes. This leads to a variation in conductance, hence, an interfacial memristor.[69,70] The switching between low and high conductance state, which is the mechanism responsible for memristive behavior, can also be achieved by the formation and dissociation of Bjerrum ion pairs—ionic pairs (dipoles) formed from the association of oppositely charged ions in a solution—under low and high V_{app}, respectively.[18,29,73] An anisotropic field effect of ions is generated under strong spatial ionic confinement, where ion pairs that are parallel and perpendicular to the direction of electric field are, respectively, affected by the intensity of electric field and the Debye length. The resulting ion pair clusters formed self-dissociate with slow kinetics into free ions under an oscillating electric field, inducing history-dependent conductance.[23] Fig. 5(c) describes a typical structure of a nanofluidic memristor that operates based on Bjerrum ion pairs based on two-dimensional nanochannels of molybdenum disulfide and graphite flakes.[74] Finally, the hysteretic conductivity behavior and synapse-like functionality of a fluidic memristor can also originate from the adsorption of ions to a charged surface, which leads to longer ionic retention time and slow down ion equilibrium beyond the diffusion timescale.[18] This can be realized by decorating the inner surface of glass nanopipettes or funnel-shaped polyethylene terephthalate (PET) nanochannels with polyelectrolytes, e.g., polyimidazolium, poly-l-lysine, as shown in Fig. 5(d).[21,27,75] This memory-generating mechanism is also applied to a conical nanochannel containing a mixture of ionic liquid and water, where the adsorption and desorption of cations from the ionic liquid onto the surface of a negatively charged nanochannel surface occur.[76] The manipulation of operating parameters (scan rate/frequency, signal amplitude, electrolyte concentrations, and types) and structural parameters (channel size and surface charges) enables the precise tuning of the memristive performance of these fluidic memristors.

D. Recent advances in fluidic memristors for neuromophic applications

The ability of fluidic memristors in regulating ion transport hysteresis paves the way for mimicking the synaptic plasticity of the brain and developing artificial neural networks that can be implemented in neuromorphic computing systems with greater learning speed and processing power. A PDMS microchannel filled with silk fibroin gel was used as a bioinspired resistive memory device. Based on the multistate resistive switching behavior rooted from the movement of oppositely charged ions to their respective electrodes under an applied bias, the device demonstrated spike rate-dependent plasticity with a decrease in current, from 800 to 380 μA, throughout repetitive signal pulses. Its synaptic performance was stable, as indicated by a similar change in current, despite the prolonged number of pulses. Furthermore, it also displayed similar behavior of forgetting human memory based on the slow transition from high to low resistance states, as evidenced by gradual increase in current over time. By applying presynaptic and postsynaptic spikes, the device successfully performed time-dependent spike plasticity rules such as antisymmetric

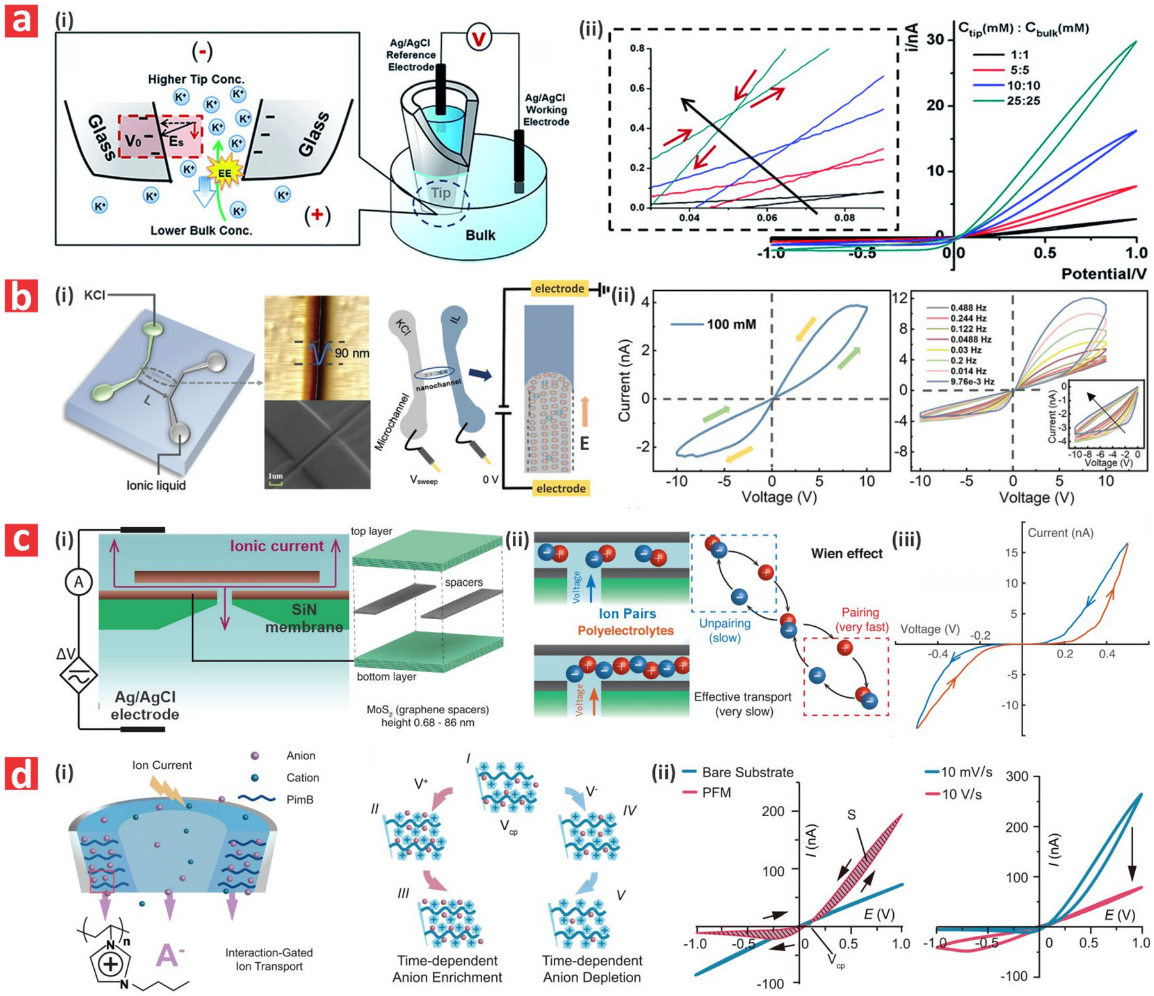

FIG. 5. Representative examples of fluidic memristors of different materials and architectures. (a) A representative memristive system based on ion concentration polarization: (i) setup of a fluidic memristor with quartz nanopipette with 60 nm radius subjected to KCl electrolyte and Ag/AgCl as electrodes; (ii) representative *I–V* hysteresis profiles in various concentrations of KCl at a scan rate of 100 mV s^{-1}. Reprinted (adapted) with permission from Li *et al.*, Chem. Sci. **6**, 588–595 (2015). Copyright 2015 Royal Society of Chemistry.[37] (b) A representative nanochannel-based interfacial memristor: (i) schematic showing a PDMS substrate with embedded microchannels and a centered nanochannel, where ionic liquid and KCl electrolyte are used to form an immiscible interface; (ii) pinched *I–V* curves of fluidic interfacial memristor due to electroosmotic flow effect-induced hysteresis and the effect of sweep frequencies (0.005–0.25 Hz) on the hysteretic loops. Reprinted (adapted) with permission from Chen *et al.*, Adv. Electron. Mater. **7**, 202000848 (2021). Copyright 2021 John Wiley and Sons.[72] (c) A representative two-dimensional synaptic nanofluidic channels: (i) nanofluidic memristive system based on molybdenum disulfide (MoS_2) separated by graphene spacers; (ii) illustration shows the memristor effect of the proposed device arisen from Wien effect and the associated formation and breakdown of Bjerrum pairs; (iii) the resulting *I–V* curve displayed a loop that is pinched at the origin. Reprinted (adapted) with permission from Robin *et al.*, Science **379**, 161–167 (2023). Copyright 2023 The American Association for the Advancement of Science.[74] (d) A representative example of polyelectrolyte-confined fluidic memristor (PFM): (i) schematic illustration of a glass nanopipette with inner surface polymerized with polyimidazolium brush; (ii) schematic illustration of time-dependent ion redistribution process inside PFM at different potentials due to confined polyelectrolyte–ion interactions. Reprinted (adapted) with permission from Xiong *et al.*, Science **379**, 151–161 (2023). Copyright 2023 The American Association for the Advancement of Science.[27]

Hebbian and antisymmetric anti-Hebbian learning rules. Using the current responses in terms of pulse width, amplitude, polarity and number as database, a convolutional neural networks simulation was performed by analyzing the device conductance for CIFAR-10 image recognition and a maximum accuracy of ∼90.2% was achieved.[77]

In Fig. 6, a two-terminal microfluidic memristor was built based on a quartz capillary functionalized with 1,3-dimethylimidazolium nitrate ([MMIm][NO_3]:H_2O) as ionic liquid-based resistance medium. It exhibited hysteresis and NDR effect. The application of positive potential disrupted the uniform distribution of ions within the memristor due to the accumulation of ionic charges and the enhancement of the EDL at the interface from the redox reactions that occurred at the electrodes. The spike-rate dependent plasticity (SRDP) of the memristor was assessed by applying electrical pulses with varied durations, and distinct potential amplitudes and signal forms. The neurosynaptic simulation performance of the device was well-aligned with

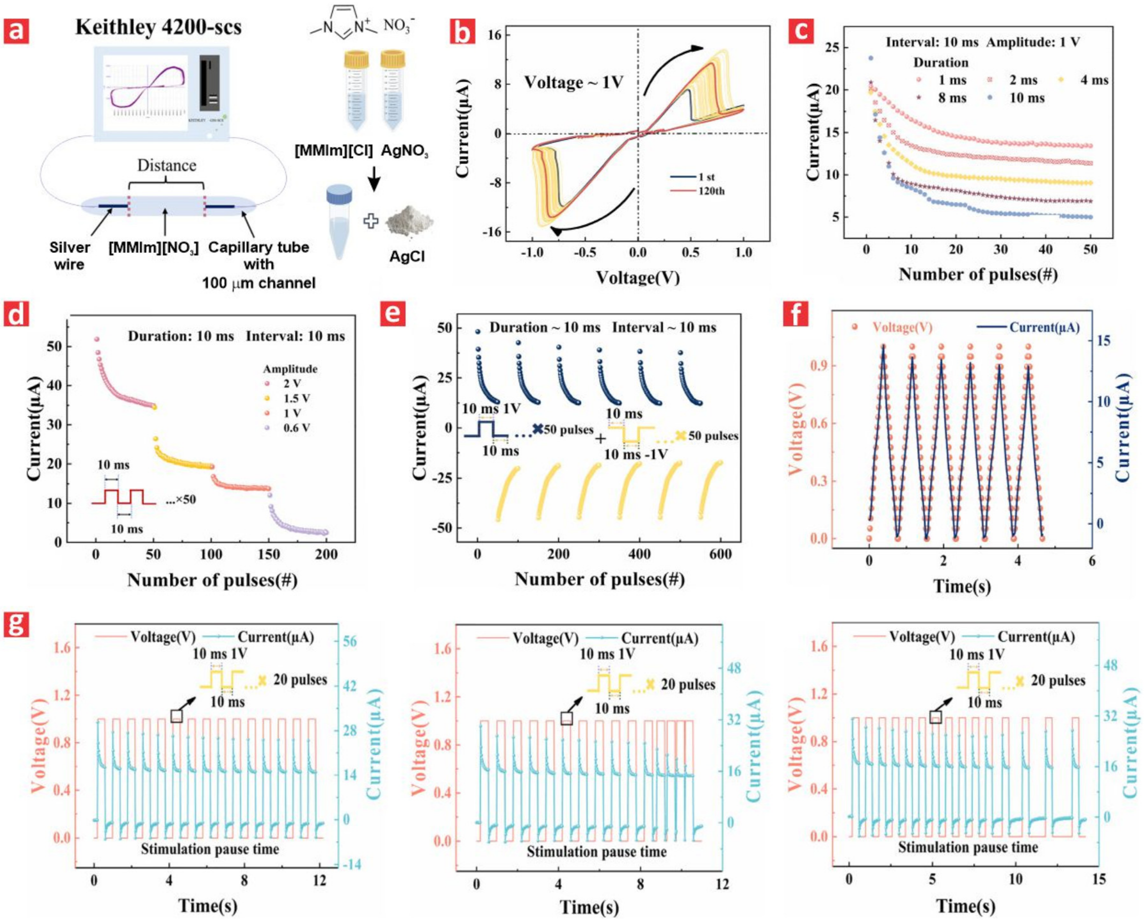

FIG. 6. Ionic liquid-based microfluidic memristor as artificial neural synapse. (a) Schematic diagram of a two-terminal memristor comprising a quartz capillary with 1,3-dimethylimidazolium nitrate ionic liquid (IL) and the resulting (b) *I–V* profile with a pinched hysteresis loop; the modulation of plasticity features of the proposed memristor by pulse stimulation with (c) voltage pulse duration (1 to 10 ms) (d) voltage pulse amplitudes (2, 1.5, 1, 0.6 V) (e) continuous rectangular pulses of amplitude of ± 1 V, (f) triangular voltage pulses with positive polarity. (g) The modulation of gap time between adjacent set of stimuli of 20 pulses (top–constant gap, middle–shrinking gap, and bottom–growing gap) to emulate habituation and recovery behavior. Reprinted (adapted) with permission from Guo *et al.*, J. Phys. Chem. Lett. **15**, 2542–2549 (2024). Copyright 2024 American Chemical Society.[78]

biological plasticity behavior and habituated learning pattern: (i) the postsynaptic currents decreased gradually under a continuous stimulation of alternating negative and positive pulses; (ii) the response to later stimuli is weaker than the preceding ones when 50 consecutive pulses were applied, but returned to the original state when the potential polarity was switched; and (iii) the decaying rate of postsynaptic current was influenced by the pause time between each adjacent set of stimuli.[78]

A different type of ionic liquid, 1,3-dimethylimidazole chloride ([Mmim][Cl]:H2O), was used to infiltrate a quartz capillary tube through self-inhalation, and copper wire electrodes were then inserted at both ends of the tube, for the preparation of two-terminal memristor with resistive memory properties. Driven by chemical reaction and ion polarization and transmission, the device displayed pronounced hysteresis loops with resistive switching and NDR effects in its *I–V* curves at optimized electrode distance and V_{app}. Note that the memristive cross-point potential of the device is at nonzero points and this indicates the contribution of capacitive effect from the migration and accumulation of ions at the electrode surface under an electric field applied to the memristor. The continuous enrichment of ionic charges at the ionic liquid–electrode interface led to an enhancement of the EDL that eventually created a limiting region of resistance and saturation current, generating a NDR effect. The biomimicking synaptic plasticity of the device was demonstrated by the current change in response to a train of six voltage pulses of varying pulse shape, width, amplitude, and frequency, which were associated with stable and repeatable habituation behavior and spike rate dependence plasticity for temporary memory of learning progress.[79]

Based on the mechanism of ion concentration polarization for memory effect, an iontronic bipolar memristor was used to realize ionic memory and neuromorphic signal processing. Three types of polyelectrolyte gels were patterned sequentially within the microchannels formed between two glass slides: (i) anionic-selective pDADMAC (N gel); (ii) nonselective poly(ethylene glycol) diacrylate (pPEGDMA)

(M gel); and (iii) cationic-selective poly(2-acrylamido-2-methyl-1-propanesulfonic acid) (pAMPSA) (P gel). The M gel region is crucial in facilitating effective ionic modulation via in-channel ion concentration polarization (ICP) because it has significant electrical resistance stemmed from its narrow microchannel width. When a forward voltage bias was applied, both cations and anions moved toward the central M gel region from the interfacing P and N gel microchannels. This increased the ionic conductance of the microchannels due to an enrichment of ions in the M gel region, switching the memristor to its ON state. The movement of cations and anions were reversed, i.e., driven away from the M gel region, when the applied bias was reversed. An ionic depletion region with high resistance was created within the M gel, which caused the bipolar memristor to be at its OFF state. The bipolar memristors featured pronounced pinched hysteretic loops at optimal I–V scan rates and the produced memory effect was attributed to the dynamic resistance switching of the M gel from ion concentration polarization effect. The time-dependent ionic response of the system was further theoretically optimized in terms of channel length and width, polyelectrolyte gel length and space charge molar density, and electrolyte concentrations, enabling a scalable memory time from 200 to 4000 s. The potentiation and depression dynamics of the bipolar memristor were assessed based on their response to a step voltage, which yielded an Ohmic current jump that increased over the duration of the applied step voltage. This was further validated by measuring the change in ionic current and conductance in response to a train of voltage pulses.[80]

A polymer-based microfluidic device was fabricated to emulate chemical synapses and their signaling processes. Poly(diallyl-dimethylammonium chloride) (pDADMAC) cationic (n-type) polymer and poly(3-sulfopropyl acrylate) (pSPA) anionic (p-type) polymer were used to form a heterojunction with strong electrostatic interactions. The ionic current response of the device was controlled by the introduction of acetylcholine (AChCl) solution that acted as chemical stimuli into the ionic p–n junction. Upon AChCl injection, ACh^+ and Cl_- ions were absorbed by pSPA and pDADMAC polymers, respectively. The neutralization of fixed surface charges by the injected ions consequently created a depletion region in the polymer junction, facilitating the flow of ions through the polymer membrane. The device exhibited spike-generation characteristics, where the injection of AChCl polarized the polymer membrane with a rapid increase in potential from −10 to 10 mV. The potential returned to its original state upon depolarization. These potential spikes were also produced in response to consecutive AChCl injections that simulate multiple stimuli. To mimic co-induced multiple neural networks for "cooperative" synapse response, AChCl solutions were simultaneously injected into the ionic junction. Upon this stimulation, the electrical potential of the device surged over the threshold value, and this triggered a postsynaptic signal. The initiation of postsynaptic signals was determined to be influenced by the time interval between injections, with the optimum range within <10 s. The proposed microfluidic device with a p–n polymer junction has demonstrated its potential use in brain-inspired computing systems based on the conversion of chemical-to-electrical signals through charge neutralization.[81]

Using the same polyelectrolytes, n-type pDADMAC and p-type pSPA, they were photopolymerized inside glass channels to construct a microchip-based iontronic diode with memory effect. The history-dependent ion transport of this two-terminal bipolar-membrane-based ionic diode was generated from the formation or dissolution of ionic precipitate at the ionic junction between pDADMAC and pSPA. In this case, barium chloride ($BaCl_2$) and sodium sulfate (Na_2SO_4) were used as precipitating reservoir solution for p- and n-type polyelectrolyte, respectively. When a forward bias was applied, the accumulation of barium and sulfate ions from the electrolytic reservoirs at the ionic junction to form barium sulfate ($BaSO_4$) as physical blockage reduced the ionic conductivity of the memristive diode and hence ionic flow was impeded. This was quantified by a decrease in the associated ionic current, which then remained constant over time despite the effort of replacing the reservoir electrolytes with inert KCl solution to dissolve the precipitate—a phenomenon similar to long-term depression (LTD) in the nervous system. In contrast, the application of a reverse-bias voltage drove barium and sulfate ions away from the ionic junction and the precipitates were dissolved partially and temporarily. The resulting change in the polyelectrolyte network created a path for ionic flow and the diode conductivity increased momentarily, emulating short-term potentiation (STP). Short-term depression (STD) was achieved by switching the bias from negative to positive to regenerate the precipitates with a decrease in ion conductivity. Both STD and LTD were characterized by a hysteretic current bulge under the subsequent forward bias in the voltage scan in the reverse-bias region. The short-term plasticity property of the memristive diode was further evaluated through the modulation of the reverse-bias input voltage pulse amplitude, width, and interval. The gradual increase in the response current to a train of reverse-bias stimuli suggested PPF behavior in the diode, whereas the gradual ionic current decay reflected a post-tetanic potentiation. To demonstrate neuromimetic ionic signal integration with plasticity, a precipitation-based iontronic synapse (PIS) with two memristive diodes with and without a preformed precipitate integrated in a microchip was fabricated. The PIS was capable of performing potentiation and depression based on the response currents with $+0.5$ V test pulses between each input signal of a series of ± 1 V pulses, due to the nonlinear and time-dependent nature of the system. Additionally, the implementation of multiple PIS with excitatory and inhibitory configurations generated ionic postsynaptic currents that could be integrated into a total "dendritic" current as a function of time and input history, similar to the hippocampal neural circuit.[82]

Another type of polyelectrolyte, polyimidazolium brush (PimB), was grown onto the inner wall surface of glass micropipettes and nanopipettes by surface-initiated atomic transfer radical polymerization for the fabrication of a model polyelectrolyte-confined fluidic memristor (PFM). As PimB has a high charge density and anion-selectivity, chloride ions (Cl^-) from electrolytes were attracted to the polyelectrolyte layer via strong electrostatic interaction under positive bias. This caused a slow diffusion dynamics of Cl^- and hence prolonged anion enrichment in the PimB layer from the rest state to reach steady ion distribution under an applied bias. This was reflected in a gradual increase in ionic current to its steady state. Cl^- ions were then depleted at a slow kinetics in the PimB layer when a negative bias was applied, as depicted by the gradual decrease in ionic current. Therefore, the slow diffusion dynamics of anions across the PimB layer contributed to the time-dependent ionic memory. The resulting memristive fingerprint of PFM was described by its pinched I–V curves with a nonzero cross-point potential, which was found to be dependent on the voltage scanning frequency. A current increase that corresponded to paired-pulse facilitation (PPF) and a current decrease that depicted paired-pulse depression (PPD) were observed when paired voltage pulses at ± 2 V were applied to PFM. The ability of PFM to emulate STP electrical pulses was attributed to ion concentration polarization in the PimB layer induced by applied biases as the slow anion diffusion kinetics briefly retained the polarized state, i.e., strong interactions between PimB and Cl^-, despite the removal of electric field at pulse intervals. The change in conductance and current response associated with the hysteretic ion redistribution in PFM as a function of the voltage pulse interval revealed the retention time of PFM to be ∼500 ms, which is comparable to those of biological STP. Furthermore, the energy consumption of the nanopipette-based PFM was estimated to be 0.66 pJ per spike at a voltage stimulation of ∼100 mV and interval of 10 ms. The ability of the PFM to mimic dynamic filtering functions of sensory neurons was also established through its frequency-dependent conductivity based on the current response to a negative pulse train with frequencies ranged from 1 to 100 Hz. The PFM also demonstrated chemical-regulated STP by tuning PimB–anion interactions, which was evaluated from its hysteretic *I–V* curves, PPF, and PPD produced in different electrolyte solutions, e.g., NaCl, $NaBF_4$, and $NaClO_4$. Among the three electrolytes, there was an increase in free Cl^- ions available for hysteretic ion redistribution to form PimB–Cl complex since Cl^- has a higher hydration energy. This modification induced a stronger memristive effect with longer retention time than those of BF_4^- and ClO_4^-. The chemical–electrical signal transduction of PFM was realized by introducing a chemical stimulus, i.e., ClO_4^-, into the inner solution of PFM. This triggered a responsive electric pulse that was analogous to a neural spike, since the depletion of anions in the PimB layer was obstructed by the decrease in effective surface charge density generated from the formation of PimB–ClO_4^-. This emulated the opening of postsynaptic ion channels activated by neurotransmitters. The induced current pulse showed a typical spiking latency behavior with a time lapse between stimulation and neuromorphic spikes. This functionality potentially could be used for encoding chemical stimulations with spike timing. As Cl^- ions moved across PFM by electroosmotic flow and electrophoresis, PimB–ClO_4^- dissociated and the current dropped to the initial state, imitating the clearance of neurotransmitters. With the versatile neuromorphic functions of the proposed PFM, this work by Xiong *et al.*[27] has contributed significantly to the development of fluidic memristors for brain-like computing.

A PDMS fluidic system comprising a channel with nanoscale width and height in between two micrometer-sized chambers was designed as a synapse-mimicking interfacial memristor. When KCl and 1-butyl-3-methylimidazolium hexafluorophosphate ($BMIMPF_6$) ionic liquid (IL) were injected into the chambers, an immiscible interface was formed between the two electrolytes. The memristive characteristic of this system was attributed to the presence of weak electrical force within the electrolyte acting on the interface of KCl–IL when the direction of sweeping potential was reversed. The pinched hysteresis loop generated described a nonlinear *I–V* correlation and conductance switching, which was optimized in terms of KCl concentration and potential sweep frequency. The analog conductance switching behavior of this artificial synapse was examined through a series of applied SET and RESET voltage pulses, where the resulting conductance change corresponded to long-term potentiation and depression with a good endurance and retention property, and diminished nonideal factors (e.g., asymmetric nonlinearity factor, nonlinear parameter, and cycle-to-cycle variation). The proposed nanochannel synapse was able to perform handwritten digit-recognition task through convolutional neural network simulation with 94% accuracy.[28,72]

Based on a similar device architecture and material, an interfacial fluidic memristor was constructed based on the bonding of PDMS molded with a funnel nanochannel and two microchannels to glass, as depicted in Fig. 7. As the selected electrolytes, namely, KCl and $BMIMPF_6$ IL, were immiscible, they formed a liquid–liquid interface at the tip of the funnel nanochannel. Its memristive characteristic was described by the *I–V* curves featuring two hysteretic current loops, where the ionic current increased and decreased upon a forward and backward scan, respectively, with a larger current value during backward scan than that of forward scan at equivalent voltages. The hysteresis in ionic transport was attributed to the asymmetric ion transfer process across the liquid–liquid interface during positive and negative scans. The synaptic plasticity of this system was demonstrated through its multistage conductance variation modulated by electrical signals, which inferred short-term potentiation and depression. The conductance change, i.e., synaptic weight, was further enhanced by tuning the signal pulse amplitude, pulse interval, and the concentration and type of electrolyte. The proposed interfacial memristor was capable of emulating Hebbian learning, as shown by conductance-based spike-time-dependent-plasticity. An increase in memristor conductance simulating the enhancement of synaptic connections was triggered when a presynaptic neuron spike (negative pulse potential) was applied before a postsynaptic neuron spike (positive pulse potential). Furthermore, the short-term learning ability of the device was manifested through SRDP. To mimic the spikes of presynaptic neurons, pulses of varied frequencies were applied. This alteration in pulse frequency resulted in varied rate of weight change, where a higher frequency yielded a faster rate in weight change. The operating voltage of this device was determined to be 200 mV with a time constant of 144 ms, indicating its comparable performance to that of biological synapses.[31]

The addition of nanoparticles into electrolytes is reported to be an effective method to enable memristive behavior of a nanochannel-based fluidic system. This can be done by adsorbing silicon dioxide nanoparticles (SiO_2–NP) on the inner surface of the tip of poly(ethylene terephthalate (PET) conical nanochannel by electrophoresis. The history-dependent pinched hysteresis of SiO_2–NP-adsorbed nanochannel was caused by the conductance variation arise from the elastic strain at the polymer nanochannel tip, which was induced by the electrical force of negatively charged SiO_2–NP. The memory effect was clearly indicated by the pinched hysteresis loops in its *I–V* curves, with anti-clockwise current loop at positive bias voltage caused by increasing conductance, and clockwise loop with minimal conductance under negative bias. The current hysteresis was investigated under a systematic variation of parameters such as KCl electrolyte concentration and pH, size of SiO_2–NP, type of nanoparticles, scanning frequencies and scanning voltage amplitude. It is interesting to note that the current hysteresis diminished when the pH of the KCl electrolyte was close to the isoelectric point of SiO_2–NP due to the inability of the neutral nanoparticle to impose strain. To demonstrate SRDP, periodic stimulating voltages with a time interval of 0.1 s were applied. The corresponding current increased rapidly followed by a saturation with a conductance fourfold higher than that of the initial state. In contrast, the change in conductance was negligible when the time interval of the spike voltages was prolonged to 9 s. The forgetting process, which is

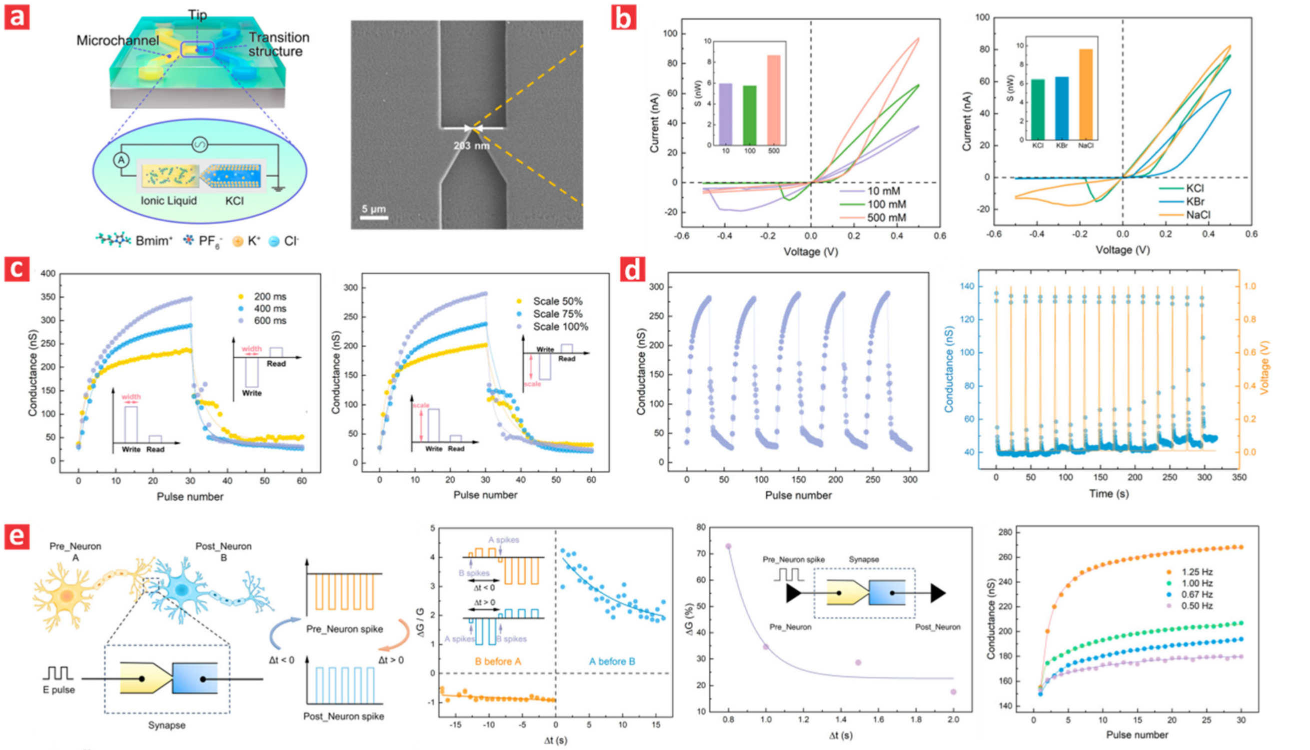

FIG. 7. Funnel nanochannel memristor as artificial synapse. (a) Illustrative diagram of funnel-shaped nanochannel with liquid–liquid interface formed between KCl electrolyte and 1-butyl-3-methylimidazolium hexafluorophosphate IL, with SEM image (right) revealing a tip width of 203 nm. (b) The modulation of hysteresis loops by varying KCl concentration (left) and electrolyte type (right). (c) Time-dependent conductance change under different pulse width (left) and amplitude (right). (d) Time-dependent conductance change, endurance and consistency when the device is subjected to consecutive pulse cycles (left) and large pulse intervals (right). (e) Demonstration of Hebb's law through STDP by applying pulse sequence (top) and (SRDP) by applying pulses of varied frequencies (bottom). Reprinted (adapted) with permission from Li *et al.*, Nano Lett. **24**, 6192–6200 (2024). Copyright 2024 American Chemical Society.[31]

related to Hebbian learning, was depicted by the exponential decrease in postsynaptic current to its initial state in response to stimulating depressing spikes. This was also correlated with long-term potentiation and depression when periodic consecutive potentiating and depressing voltage pulses were applied. The SRDP characteristic of the system was further established by the conductance change, i.e., exponential decrease in synaptic weight, under paired-pulse facilitation as a function of potentiation pulses with a spike interval of Δt.[83]

The integration of microbubble in a microfluidic system has been demonstrated to function as soft memristor based on the tuning of water film thickness between a bubble and solid surface by an external electrical field. The proposed microfluidic device comprised of two microchannel layers sandwiching two PET membranes: one track-etched with nanochannels while one laser-drilled with micropore, and a nematic hybrid liquid crystal microbubble is introduced on the top of microchannel layer to create a thin liquid film between the bubble and PET membrane with nanochannels (Fig. 8). Governed by the flow kinetics and film thickening–thinning dynamics, it displayed current hysteresis in its I–V profiles measured in 0.2 M NaCl with addition of sodium dodecyl sulfate (SDS) at increasing scanning periods, with counterclockwise and clockwise hysteresis at negative and positive bias, respectively. However, the hysteresis disappeared at too high scanning period with a sudden drop of conductance at positive bias due to the reset of film thickness from liquid flow through the bubble boundary. Due to the pressure-driven flow caused by electrostatic forces on the negatively charged liquid–vapor interface, the water film became thicker from the repulsion at negative V_{app} and electroosmosis; and thinner from the attraction at positive biases. The microbubble-based soft memristor was also used to emulate adaptive learning as in synapses. By applying potential spikes with a 5 V amplitude, 200 ms duration, and a 100 ms interval, the synaptic weight change in both PPF and post-tetanic potentiation (PTP) decreased exponentially. When the stimulation spikes were changed in terms of pulse width, and intervals, the conductance change decreased gradually with increasing interval, which showed a SRDP characteristic. Furthermore, the effect on synaptic weight was only significant when the stimulating pulse amplitude exceeded a threshold amplitude of 1 V. The good learning-experience of the proposed soft memristor was validated by the exponential decay of conductance with an average time of 1.3 s, and its proportionality to the number of voltage spikes.[84]

A similar microdroplet-based memristor also shows potential as reconfigurable neuromorphic computing (Fig. 9). The proposed system showed the clockwise pinched hysteresis at positive V_{app}, which represents negative differential resistance effects. This resistance

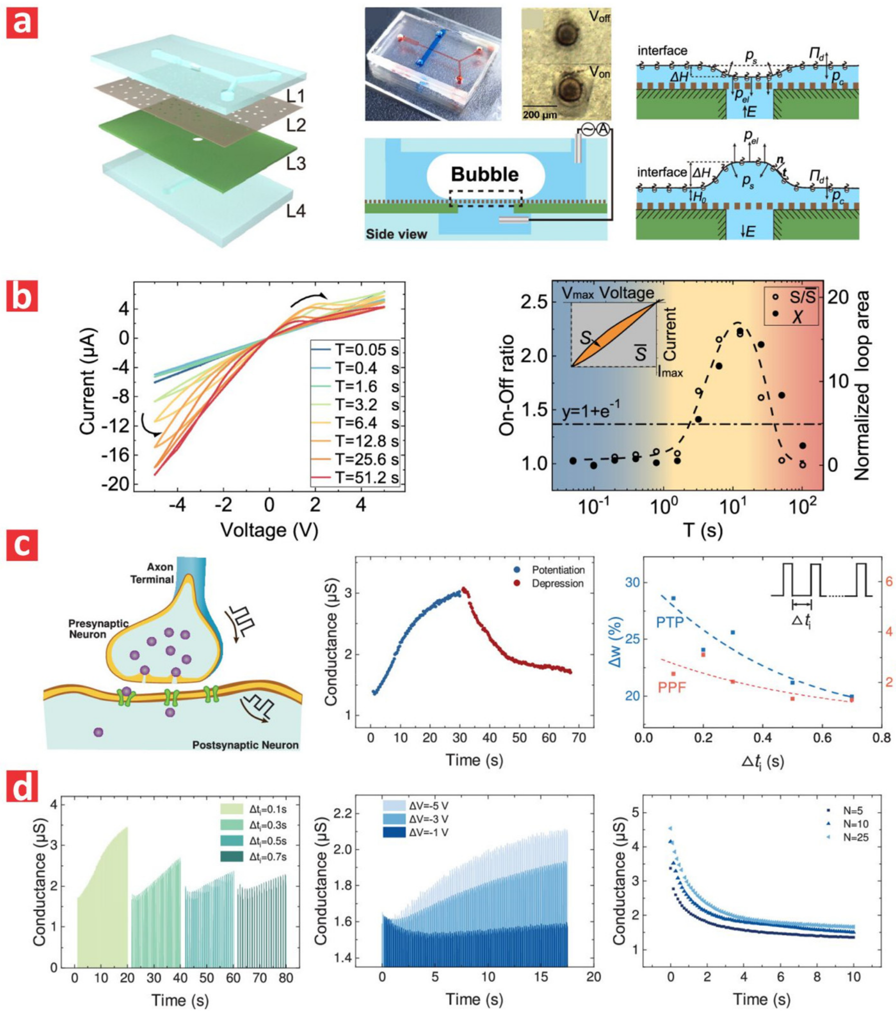

FIG. 8. Microdroplet-based soft memristor based on liquid–vapor surface of a microbubble. (a) Fabrication of microfluidic chip containing layers of PET membranes patterned with microchannels, nanochannels, and micropore, with a schematic illustrating film thinning and thickening process under an applied bias. (b) Memristive characteristics in terms of *I–V* curves, on–off ratio, and hysteresis loop areas in 0.2 M NaCl with SDS added at critical micelle concentration. (c) Synaptic characteristics in terms applied voltage polarity modulated conductance change (middle) and time pulse modulated synaptic weight (PPF and PTP) (right). (d) Synaptic characteristics in terms of conductance change modulated by time interval, pulse amplitude and number of potentiated spikes. Reprinted (adapted) with permission from Niu *et al.*, Nano Lett. **24**, 102202 (2024). Copyright 2024 American Chemical Society.[84]

change is attributed to voltage-induced deformation of liquid–liquid interface caused by Maxwell stress under an electrical field. The synaptic plasticity of the system was characterized by (i) SRDP with a minimum conductance based on periodic voltage spikes of various time interval; (ii) PPD with an increase in synaptic weight as a function of time interval; (iii) LTP and LTD with an exponential decrease in conductance with potentiation spikes, which recovers with depression voltage spikes. Using a thermotropic liquid crystal and coupled with Peltier chip for temperature control, the system could mimic animal season hibernation accompanied by change of neuronal activity. The conductance response, i.e., decrease in synaptic weight, to stimuli spike trains encoded from a 28×28 pixel handwritten image was demonstrated to decrease at lower temperature, which aligns with reduced neural activity at colder environments. The temperature-responsive characteristic of the system was also used to train artificial neural network (ANN) of 784 input pixels, 200 neurons in hidden layer, and 10 output neurons, which revealed a better recognition accuracy at higher temperature, similar to heightened neural activity at increased temperature displayed by animals.[85]

Through surface functionalization, the ion concentration polarization effect induced by ion migration across a single nanopore can be harnessed to regulate the ionic conductivity for memory effect. Ling *et al.* constructed positively and negatively charged single-pore nanofluidic memristors by modifying the inner surface of glass nanopore with (3-aminopropyl) triethoxysilane (APTES) and tannic acid, respectively. Due to the difference in their surface charges, the direction of hysteresis loops of the nanofluidic memristors opposed each other. This implied that the ionic conductivity of the APTES-modified nanopore increased but that of the tannic acid-modified nanopore decreased upon an applied positive bias because of the reversal of ion enrichment/depletion within the nanopores generated from the opposite surface charges. The functional groups available on the surface of the nanopores provided sites for protonation/deprotonation, and the ionic conductivity of the nanofluidic memristors could be modulated based on the degree of protonation to emulate the dynamic transition from silent synapses to excitatory or inhibitory synapses. By applying two consecutive positive voltage pulses, the ratio of current change corresponding to paired-pulse facilitation for APTES-modified nanopore

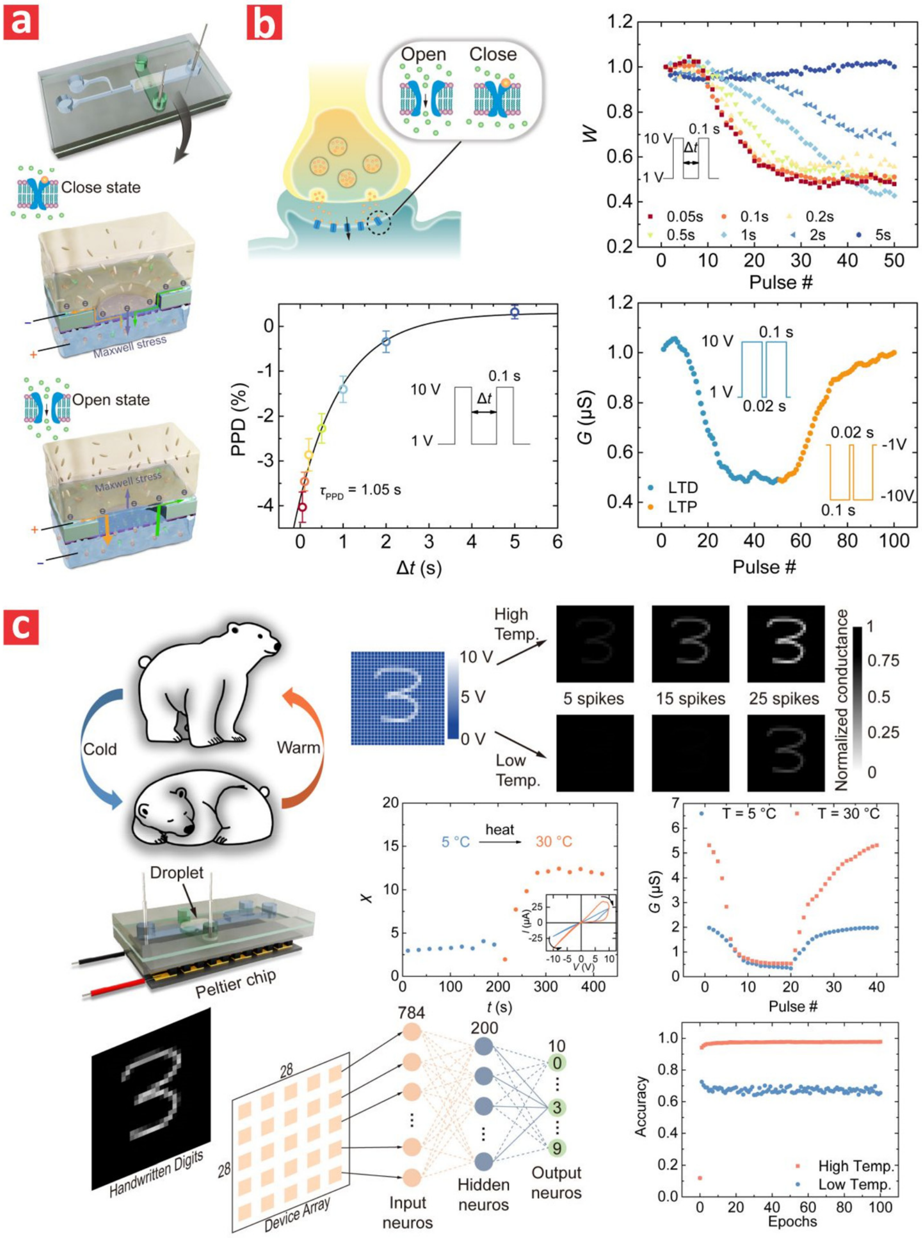

FIG. 9. Microdroplet-based soft memristor based on liquid–liquid surface of a liquid-crystal microdroplet. (a) Illustrated microfluidic system by integrating two membranes with a microwell and nanochannels each in between two layers of PDMS microchannels. (b) Adaptive learning features characterized by SRDP, PPD, and LTD and LTP. (c) Temperature-modulated memristor mimicking neuronal activities responding to external stimuli based on conductance response to encoded visual signal and its recognition accuracy. Reprinted (adapted) with permission from Ma *et al.*, Cell Rep. Phys. Sci. **5**, 102202 (2024). Copyright 2024 Authors; licensed under a Creative Commons Attribution (CC BY) license.[85]

increased from the ion enrichment process via protonation, whereas the depletion of ions in tannic acid-modified nanopore decreased the conductivity with an increase in current change ratio related to paired-pulse depression. Not only the writing and erasing ability of APTES-modified nanopore was established by the change in conductivity under the influence of the polarity of applied voltage pulse but also the spiking-rate-dependent plasticity was validated by the decrease in conductivity change with increasing time intervals between input pulses. To show the potential of these nanofluidic memristors for brain-like computing, they were integrated into reconfigurable logic gates with positive and zero voltage pulses, respectively representing input "1" and "0," and the resulting high and low conducting states corresponded to output "1" and "0." The conductivity outputs of these nanofluidic logic memristors were tuned by pH, realizing OR, AND, NAND, and NOR logic gates. By combining these nanofluidic memristors in different configurations, an artificial nanofluidic neural network for matrix multiplication was created with the underpinning basis of cooperative interaction of these artificial synapses. The connection of two nanofluidic memristors in the same direction, either parallel or series, retained the memristive properties but the memory effect was lost when they were connected in opposite directions.[61]

Figure 10 describes the confinement of PEDOT:PSS within a glass nanopipette for the realization of various electrical pulse patterns, e.g., PPF, PPD, SRDP, and spike-timing-dependent-plasticity (STDP). The ionic hysteretic origin of this polymer-filled nanofluidic memristor was attributed to the reversible redox and capacitive effect of PEDOT:PSS membrane, which resulted in pinched loops at near 0 V with a clockwise/anticlockwise trend in its respective first/third quadrant of the I–V profile. On one hand, a positive V_{app} induced an enhancement in ion concentration polarization, therefore, a time-accumulated polarization effect was observed in the range of 0 to 1 V. On the other hand, depolarization occurred from −1 to 0 V scanning range due to inhibited ion concentration polarization. The correlation between the hysteresis performance and scan rates shown by the proposed nanofluidic system has revealed a Hodgkin–Huxley ion channel memristor characteristics, with sufficient ionic equilibrium and lagged ionic changes at low and high scan rates, respectively. Based on the time-dependent ionic polarization/depolarization, PEDOT:PSS confined nanopipette has demonstrated: (i) PPD and PPF upon the application of presynaptic pulses of $\pm$ 0.4 V with 10 ms duration and 20 ms interval; (ii) temporal filtering feature upon the stimulation by multiple voltage spikes of different intervals (1 to 67 Hz); and (iii) STDP and antisymmetric anti-Hebbian learning rule based on the conductance change in response to voltage spike order and interval. The derived PPD and PPF time constants of the proposed system was within several to hundreds of ms range, which is well-aligned to that of biological systems. The proposed nanofluidic synapse also demonstrated bionic spiking behavior involving transmembranous electrical dynamics under input ionic currents of $\pm$7 nA with an energy consumption of 77 pJ, which could be further electrically tuned by varying stimulus current, resting potential and time. The chemical tunability of the spiking functionality was achieved by a modulation of electrolytic cation concentrations and the addition of dopamine neurotransmitters, realizing neuronal excitability. The ionic current-induced spiking produced by the proposed nanofluidic synapse was highly analogous to that of biological action potentials with similar phases of resting potential, depolarization, and hyperpolarization, contributing to brain-like neuromorphic computation.[86]

The emergence of memory in the transport of ions across two-dimensional nanofluidic channels was investigated and used for the implementation of Hebbian learning. Two types of nanofluidic memristors with similar geometry but different surface properties were fabricated: (i) "pristine" channels formed by MoS_2 flakes with graphene nanoribbons as spacers; and (ii) "activated" channels created in between two graphite flakes with an etched trench on the bottom flake. Both pristine and activated nanofluidic memristors produced hysteresis current loops pinched at 0 V when subjected to a time-varying applied voltage. Note that the memristive effect appeared at frequencies ranging from 0.1 to 200 mHz, which was below the frequencies where capacitance-induced hysteresis occurred. The properties of the hysteretic current response were further modulated by the electrolyte concentration, pH and type, as well as the channel height. The analysis of conductance curves as a function of voltage revealed pristine nanochannels as a unipolar memristor and activated nanochannels as a bipolar memristor, as defined by their self-crossing and open conductance curves, respectively. It is suggested that, on one hand, activated nanochannels behaved as a bipolar memristors as their conductance state changed upon reversal of applied voltage polarity. Therefore, its memory effect was attributed to ion enrichment and depletion in the nanochannel facilitated by the high surface charges. On the other hand, the nonlinear response of pristine nanochannel as unipolar memristor was correlated with the formation of tightly bound Bjerrum pairs of ions under strong confinement and its associated Wien effect. As a proof-of-concept, a bipolar activated nanofluidic memristor was used to emulate Hebbian learning based on its demonstrated conductance change in response to successive voltage sweeps that corresponded to short- and long-term memory. The long-term modification of the memristor was validated through the application of 30 "write" voltage spikes (+1 V for 10 s) and 30 "erase" spikes (−1 V for 10 s). The writing spikes induced a conductance potentiation, and the conductance measured between each spike at a reading pulse (+0.1 V for 5 s) revealed no fluctuation. The erasing spike then triggered potentiation depression by resetting the conductance back to its initial state. The implementation of Hebbian learning involved the activation of neuron-mimicking nanofluidic memristors by voltage spikes. This resulted in an increase in conductance when a presynaptic spike was followed by postsynaptic spike, which resonated the strengthening of connection between two neurons. However, the conductance decreased when the order of neuron activation was reversed or the delay was prolonged, indicating weakening or unchanged neuron connections. The nanofluidic memristors produced in this work exhibited not only synaptic tunability, but also the realization of basic learning algorithms within a simple nanoarchitecture.[74]

The dimension of asymmetric channel-based fluidic memristor can be further scaled down by using heavy ion irradiation to create one-dimensional latent track as Angstrom-scale channel. This is demonstrated by Shi *et al.*, where they fabricated an asymmetric channel featuring chemically etched conical nano-opening and Angstrom channel on PET foil. The conical side of the channel was further modified with poly-L-lysine (PLL) coating to provide the structure with positive surface charges. The memristive property of the structure was attributed to the movement of PLL molecules across the Angstrom-scaled channel under an external electric field: (i) the penetration of PLL molecules into the channel under negative bias increased the resistance to ionic flow (OFF state); and (ii) positive bias drove PLL molecules out of the channel and the resistance was reduced (ON state). Therefore, the I–V curve exhibited hysteresis loops pinched at (0,0) with a high and low conductivity state at positive and negative potential, respectively. The hysteresis loop areas, which defined the memory effect, were modulated by scanning frequency and range, as well as KCl electrolyte pH and concentration through their impact on the ionic concentration polarization, change in entropy barrier for PLL molecules to penetrate and charging–discharging current of capacitance at the channel surface. The excitatory postsynaptic current (EPSC) of the Angstrom-scale fluidic memristor in response to 15 voltage spike cycles with fixed time interval reflected long-term potentiation (LTP) with an exponential increase in EPSC amplitude at one polarity, and long-term depression (LTD) at the opposite polarity with decreasing EPSC amplitude. The system also exhibited short-term plasticity (STP) based on the increasing EPSC respecting to applied paired pulses with a time interval of 25 ms. To emulate the learning–experience behavior, i.e., Hebbian learning, periodically potentiating pulses were used to stimulate the fluidic system. It was found that the synaptic weight increased rapidly and saturated with the number of pulses. However, when the potentiating stimulation was removed,

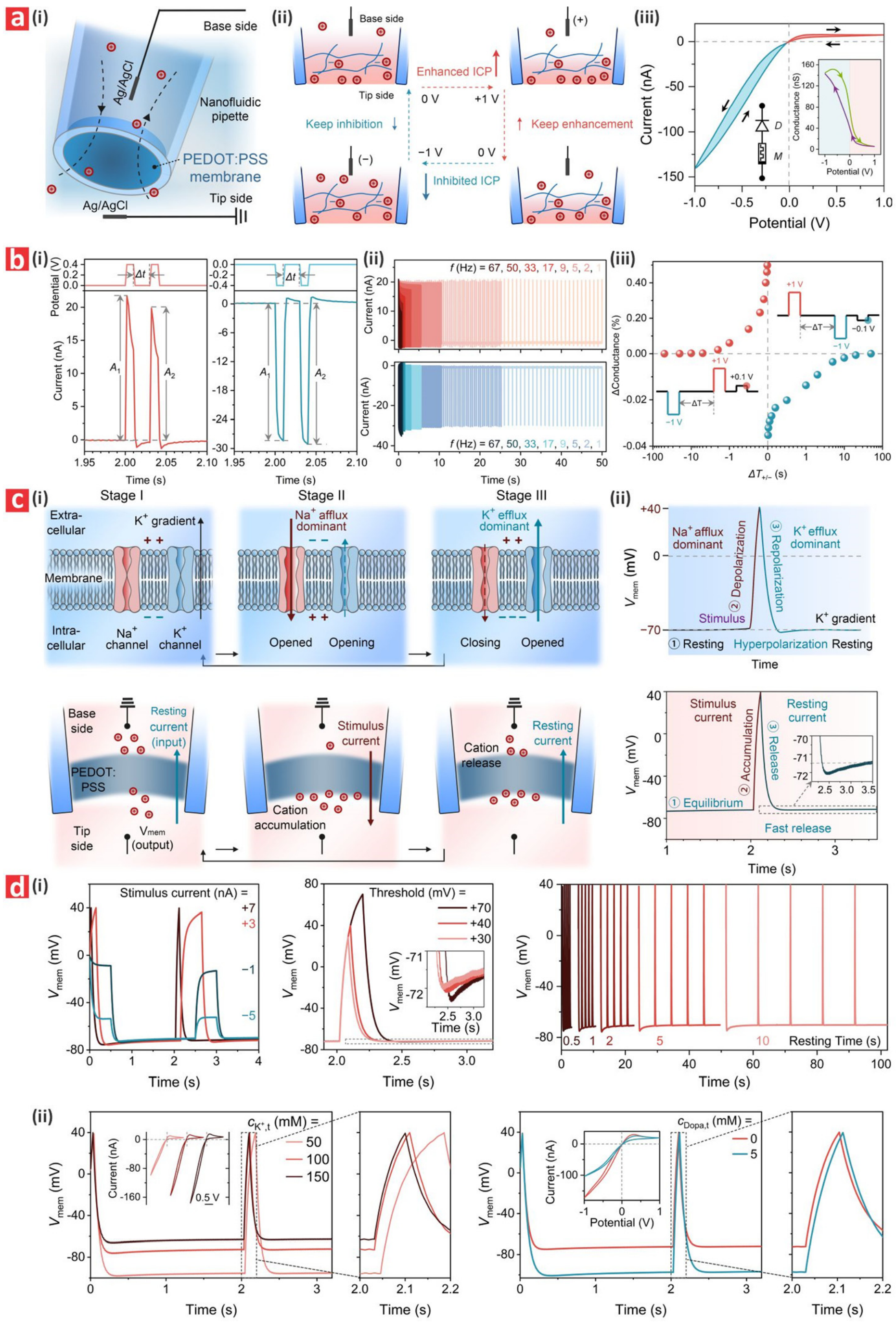

FIG. 10. Nanofluidic memristor as a synthetic spiking synapse. (a) PEDOT:PSS-based nanofluidic synapse: (i) illustrative depiction of polymeric nanopipette with a confined layer of PEDOT:PSS at the tip; (ii) descriptive diagram on the enhancement and inhibition of ion concentration polarization within nanopipette during potential sweeps; (iii) the resulting *I–V* hysteresis effect in response to the periodic triangular wave of 100 mV s^{-1} in 100 mM KCl. (b) Time-dependent synaptic plasticity with demonstration of (i) paired-pulse depression and facilitation at a time interval of 20 ms; (ii) SRDP signals under 50 consecutive pulses of $\pm$ 0.4 V intensity, 10 ms duration, and varying frequency (1–67 Hz); (iii) STDP signals with a change in conductance induced by positive and negative input pulse. (c) Demonstration of bionic spiking behavior: (i) illustrations comparing the generation of action potential in biological ion channel (top) and PEDOT:PSS artificial synapse (bottom); (ii) the corresponding transmembrane potential produced by biological (top) and artificial (bottom) synapses under input ionic currents of $\pm$ 7 nA (bottom). (d) The tuning of spiking behavior of artificial synapse by (i) electrical inputs – stimulus current (left), threshold values (middle), and spiking frequencies (right); (ii) chemical inputs – concentrations of potassium ions (left) and addition of dopamine (right). Reprinted (adapted) with permission from Xu *et al.*, Proc. Natl. Acad. Sci. U. S. A. **121**, e2403143121 (2024). Copyright 2024 National Academy of Sciences.[86]

there was an exponential decrease in synaptic weight to a value of ~60%, which is analogous to the forgetting curve of human brain. The power consumption of the proposed fluidic memristor, which was determined to be 2–23 fJ per spike, were comparable to those of biological synapses (1–100 fJ per synaptic event) but lower than that of CMOS-based brain-inspired chips (23–26 pJ per synaptic event).[75]

Likewise to single conical nanopore, a nanofluidic membrane featuring multipores exhibits versatile synaptic functions enabled by the combined effect of rectification and memristor properties with a greater current output. When a polyimide-based membrane with conical pores sized 10 and 100 nm at the tip and base, respectively, was subjected to 2 M KCl electrolyte under an applied bias, the hysteresis behavior emerged at higher signal frequency range (10–100 Hz) (Fig. 4). This is because of the presence of surface charges on the nanopore wall to promote accumulation of mobile ions, i.e., high current, at the pore tip under positive bias but depletion at negative bias (low current), which explained the greater hysteresis loop at $V > 0$ than that of $V < 0$. When the frequency was in the range of 10–100 Hz, the relaxation time characteristic of the mobile ions and nanopore surface charges was longer than the signal period, causing a delay in ion migration in response to the applied bias. The memristor behavior vanished as signal frequency went beyond 100 Hz since the speed of external signal was too fast for the mobile ions to follow. Based on the quantification of the area enclosed within the loop, the memristive performance was the best at a signal frequency of 20 Hz and it could be further optimized by manipulating signal voltage amplitude, as well as electrolyte concentration asymmetricity, type and pH. To demonstrate the synaptic tunability, their current responses to a train of 2 ms positive voltage pulses of amplitude +1 V and negative voltage pulses of amplitude −1 V were evaluated in KCl electrolyte of different pH. At pH = 3.3, no gradual potentiation was observed in the nanofluidic memristor due to their neutral surface charge. On one hand, when the pH of the electrolyte was increased to 7, the applied positive pulses induced current potentiation and synaptic depression during the negative pulses. On the other hand, an electrolyte of pH 2.2 reversed the conductance response with current potentiation occurring under negative potential pulses. The pH-tuneable synaptic potentiation and depression of the multipore nanofluidic memristors enabled reverse modulation of memory effects, which is useful for ionic neuromorphic computation.[60]

Ramirez *et al.* further extended the investigation on the memory behavior of a nanoporous polyimide membrane in symmetric and asymmetric electrolyte types and concentrations. In the case of symmetric condition, the nanofluidic membrane was sandwiched between two reservoirs of electrolytes of the same type (e.g., KCl, calcium chloride $CaCl_2$) and concentrations (e.g., 50, 100, and 500 mM). Compared to that of symmetric 50 mM KCl, the hysteretic *I–V* curve produced in symmetric 50 mM $CaCl_2$ was less rectified with a much smaller loop areas at the same potential frequency (10 Hz) and amplitude (2 V). This was attributed to the decrease in nanopore surface charges from the binding interaction between calcium ions and carboxylate ions on the nanopore surface, as well as the increased Debye screening of divalent calcium ions. This also clarified the absence of conductance potentiation and depression in 50 and 100 mM $CaCl_2$ electrolytes, and a slight potentiation with reverse polarization at 500 mM $CaCl_2$. Interestingly, a third hysteresis loop was observed when symmetric $CaCl_2$ concentration was decreased to 10 mM, which was absent in that of KCl electrolyte. Since electrostatic interaction of divalent cations has a different kinetics than that of monovalent ions, this results in different pore relaxation phenomena involving potassium and calcium ions that produce their own distinct memory characteristics. Furthermore, divalent Ca^{2+} ions might enhance the solution capacitance and this contributed to the presence of the extra central loop, which was validated by impedance spectra. To further evaluate the effect of asymmetric electrolytes, two configurations were used: (i) pore tip facing 50 mM KCl and pore base facing 50 mM $CaCl_2$; and (ii) pore tip facing 50 mM $CaCl_2$ and pore base facing 50 mM KCl. The former has shown three rectified hysteresis loops in its *I–V* curve but a less rectified and memristive single pinched loop in the latter, which is associated with the ion transport and binding behavior of divalent cations. Therefore, the former showed a more marked conductance potentiation and reset effect than that of the latter. The memory effect of these nanofluidic memristors were also studied in a multi-ionic electrolyte system composed of different ratio of KCl to lanthanum chloride ($LaCl_3$) solution. This showed rectified and linear hysteresis loops depending on pore charge inversion phenomenon from the adsorption of trivalent cation on the pore surface. This work has demonstrated the modulation of neuromorphic conductance responses by solution characteristics, which could help building ionic circuits for brain-like computing.[87]

Ramirez *et al.* also investigated in detail the effect of ionic concentration gradients on the memristive switching of nanofluidic membranes composing of ~300 polymer-based conical nanopores. The diameters of each nanopore in the membrane were 20 and 300 nm at the tip and base, respectively. When an electrolyte concentration gradient was used, i.e., nanopore tip facing higher KCl concentration ([KCl]) and nanopore base facing lower [KCl], its *I–V* curve featured rectifying pinched hysteresis loops with higher conductivity at $V > 0$ V due to enhanced ion accumulation at the pore tip. This was correlated with inductive memory effect, which diminished at higher signal frequency. The capacitive memory effect, indicated by a clockwise loop at $V < 0$ V, increased with signal frequency. Opposite memristive effect with high conductance at $V < 0$ V was achieved when the electrolyte configuration was reversed with high [KCl], providing a large ionic reservoir for ion accumulation at the pore base. The switchable ON/OFF conductance state of the nanoporous memristors was confirmed by ionic conductance and current semi-logarithmic plots, which have shown closed counterclockwise loops at $V > 0$ V and a drastic drop in conductance at $V < 0$ V. The synaptic current response of the membrane at different configuration of ionic concentration gradient was evaluated based on input spike signals of positive and negative pulses of duration of 2 ms and different amplitude (1, 2, and 3 V) in sequence. With the pore tip facing the more concentrated KCl, conductance potentiation and depression were observed with increasing significance as the pulse amplitude increased. In contrast, this synaptic behavior disappeared when the concentration gradient was reversed, which might be due to complete exclusion of anions from negatively charged nanopores. The neuromorphic-like conductance potentiation behavior with respect to spike pulses under an ionic concentration gradient further establishes the potential use of nanofluidic system as ionic memristors for neuromorphic applications.[88]

In addition to electrolyte concentration gradient, electrolyte pH gradient is another effective parameter to modulate the memristive and neuromorphic-like conductance potentiation characteristics of nanofluidic memristors. Illustrated in Fig. 11, a multipore polyimide membrane with etched conical nanopores (tip and base diameter of 20 and 200 nm, respectively) were subjected to a 50 mM KCl electrolyte pH gradient of 7 and 1.5 to tune the surface charges of the nanopores. The dynamic *I*–*V* curves of the membrane at a pH gradient featured pinched hysteresis loops, where the curve orientations were affected by the configuration of the nanopore (tip/base) facing the electrolyte of pH 7 or 1.5. The nanoporous fluidic memristors also displayed neuromorphic-like spikes in their current–time profiles under a pH gradient when 11 positive and 11 negative voltage pulses with 5 V amplitude, 2 ms duration, and 2 ms interval were applied as input. A gradual increase in conductance for positive and negative amplitudes was observed when the tip of nanopore faced KCl electrolyte of pH 7, however, the memristive nanopore system was at low conductance states when pH configuration was switched. The effect of pH configurations was also evaluated in the nanofluidic systems comprising a series arrangement of memristive nanopores. It is interesting to observe that: (i) the rectifying hysteresis loop only self-crossed when

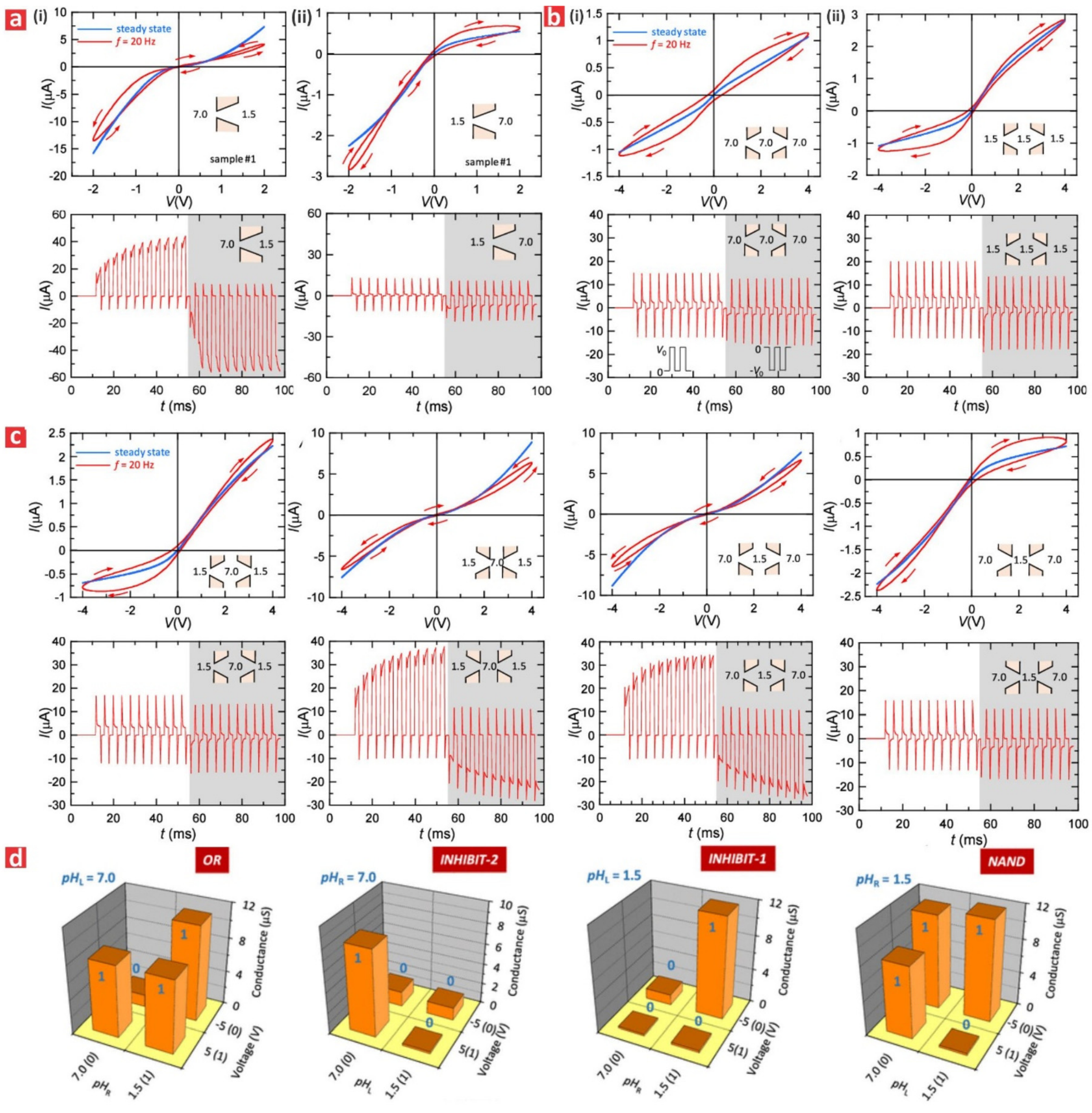

FIG. 11. Electrolyte pH-modulated memristive effect in nanofluidic memristor. (a) Electrochemical characterization of nanofluidic memristors in asymmetric pH of KCl electrolytes: *I*–*V* and current potentiation profiles of nanofluidic memristor with pore tip facing KCl of (i) pH 7.0 and (ii) pH 1.5. (b) Electrochemical characterization of two memristive nanopores connected in series subjected to symmetric pH conditions: (i) KCl pH 7.0 and (ii) KCl pH 1.5. (c) *I*–*V* and current spike profiles of two nanofluidic memristors in series in varying KCl pH and nanopore arrangement conditions. (d) Logic function responses obtained corresponding to pH of KCl and applied voltage (V_{app}) as input signals and conductance change as output signal. Reprinted (adapted) with permission from Portillo *et al.*, J. Phys. Chem. Lett. **15**, 7793 (2024). Copyright 2024 American Chemical Society.[89]

both nanoporous membranes had their pore tips facing an electrolyte pH of 7 and pore bases facing KCl pH 1.5; (ii) rectification was absent in symmetric electrolyte pH 7 condition but present in symmetric electrolyte pH 5 condition; and (iii) rectifying non-pinched hysteresis loop was produced when the nanopore tips and bases of both membranes were subjected to KCl pH 1.5 and 7, respectively. These results were also reflected in their current–time profiles, where significant synaptic potentiation in both positive and negative voltages for memristor systems with two membranes arranged in series and their pore tips facing KCl pH 7. These pH-modulated conductances of the memristive nanopores were then used as basis to implement logic functions. Based on input 1 variable as sign of V_{app} (0 for V = –5 V and 1 for V = 5 V), input 2 variable for nonfixed KCl pH (0 for pH 7 and 1 for pH 1.5), and conductance as output variable (0 for low conductance and 1 for high conductance), different logic responses, i.e., OR, INHIBIT-1, INHIBIT-2, and NAND functions, were obtained as a proof-of-concept for potential applications in iontronic neuromorphic circuit.[89]

The memristive behavior of polyimide-based multipore membrane can also be regulated based on their arrangement in a circuit, as demonstrated by Ramirez *et al.* Mutipore membranes with the same polarity that were connected in series exhibited rectified pinched hysteresis, with synaptic conductance potentiation corresponding to trains of positive spike pulses. However, only one current loop with no pinched behavior occurred when the membranes had opposite polarity in series. This was attributed to the absence of inductive behavior and the current being governed solely by the capacitive branches. This observation also aligned with the loss of conductance potentiation. Similar to the results obtained at the same polarity in series connection, nanofluidic membranes with their pore tips facing the same side connected in parallel exhibited pinched hysteresis loops with its ON state under positive bias. They also showed conductance potentiation at positive voltage pulses but not at negative voltages. Conversely, the *I*–*V* curve of nanofluidic membranes in anti-parallel arrangement, i.e., their pore tips facing different direction, featured double-pinched loop, with inductive loops at both V < 0 V and V > 0 V, and a capacitive loop at the origin. Note that the presence of conductive loops at V < 0 V and V > 0 V were responsible for the conductance potentiation observed at both positive and negative voltage pulses. Therefore, this work provided insights into the logical arrangement of nanofluidic memristors to achieve synaptic functionality for neuromorphic applications.[90]

Nanofluidic memristor featuring highly asymmetric channels (HAC) of silicon nitride, palladium, and graphite crystals with demonstrated potential for circuit-scale in-memory processing was reported by Emmerich *et al.*[55] HAC displayed a clear bipolar memristive signature with an increasing and decreasing conductance at positive and negative voltages, respectively. Other unique features exhibited by HAC include: (i) memory retention at low voltages; (ii) implementation of STDP by applying short voltage pulses; (iii) a combination of fast speed and large conductance ratio; and (iv) delayed switching (drastic conductance increase when applied voltage became positive). This shows the potential of the system for neuromorphic applications such as Hebbian learning and conditional logic as the switching ability enables the reading of memory state without interrupting programmed state. Furthermore, the integration of HAC in logic circuits with interactive devices was demonstrated. A material implication (IMP) logic gate was constructed using two parallel HACs connected to a resistor, where one functioned as P-switch with constant conduction state during logic operation and the other as Q-switch with switchable conductance state triggered by P with low conductance. The strong nonlinear dynamics of HACs and its associated conditional switching enabled the implementation of a Boolean operation, which pave the way for the development of fully liquid circuits using these nanofluidic memristive switches.[55]

Fluidic memristors based on nanochannels with short-term memory and highly volatile properties are also promising candidates for performing neuromorphic reservoir computing—a brain-inspired neuromorphic computing algorithm based on recurrent neural networks for complex temporal data analysis and prediction. In reservoir computing, the complex nonlinear network receives input signals but only the final layer of output signals is trained for recognition task. This implies that the network must be volatile so that the internal part of the reservoir forgets a state to perform further computations.[20,91,92] In Fig. 12, Kamsma *et al.* constructed a fluidic memristor constructed based on a tapered microfluidic channel with an embedded conducting network of nanochannels between colloids and two KCl electrolyte reservoirs. The fluidic device displayed a pinched hysteresis loop in its dynamic *I*–*V* curve due to transient salt concentration polarization driven by externally V_{app}. Furthermore, the neuronal short-term plasticity, i.e., facilitation and depression, of the device was assessed by the change in conductance in response to four consecutive positive and negative "write-pulses" of 5 V and –2.5 V, respectively with a duration of 0.75 s and interval of 0.75 s. The short-term characteristic of the device was further validated when the interval between pulses was longer than the typical memory retention time with the absence of cumulative conductance change. The energy consumptions of the device were determined to be $\sim$1–10 μJ for four applied 5 V write-pulses and 10–100 nJ for five applied –1 V read-pulses. These features of short-term memory and nonlinear dynamics equipped the device with reservoir computing capabilities, which was demonstrated through *in silico* classification of handwritten numbers. Based on the translation of bit-strings (0 or 1) to voltage pulses (–2.5 V or 5 V) that generated a total of 110 conductance states per image, the device with a single-layer fully connected 110 × 10 neural network as readout function and trained on a dataset of 2000 samples was capable of achieved an accuracy of 81%. The performance of the proposed fluidic iontronic volatile memristor with adjustable memory retention times was comparable to those of solid-state memristors with an accuracy of 83%–86% based on similar protocol, bringing aqueous memristive system a step closer to neuromorphic computing.[20]

III. OTHER FLUIDIC COMPUTING COMPONENTS

A. Fundamental principles

The hardware implementation of current neuromorphic systems relies heavily on CMOS transistors, as demonstrated by TrueNorth chip with 5.4×10^9 transistors integrated to mimic one $\times 10^6$ neurons and 256×10^6 nonplastic synapses.[7,93] To achieve true emulation of neurons with synaptic plasticity, a large number of transistors are required, which is impractical for conventional applications in terms of energy and size.[7] This has driven the development of ionic transistors—the fluidic analogy of voltage-gated sodium and potassium channels in biological systems, which is the main focus in among others fluidic computing components in this review.[94] Similar to biological ion channels that control ionic flow by transmembrane potential, the

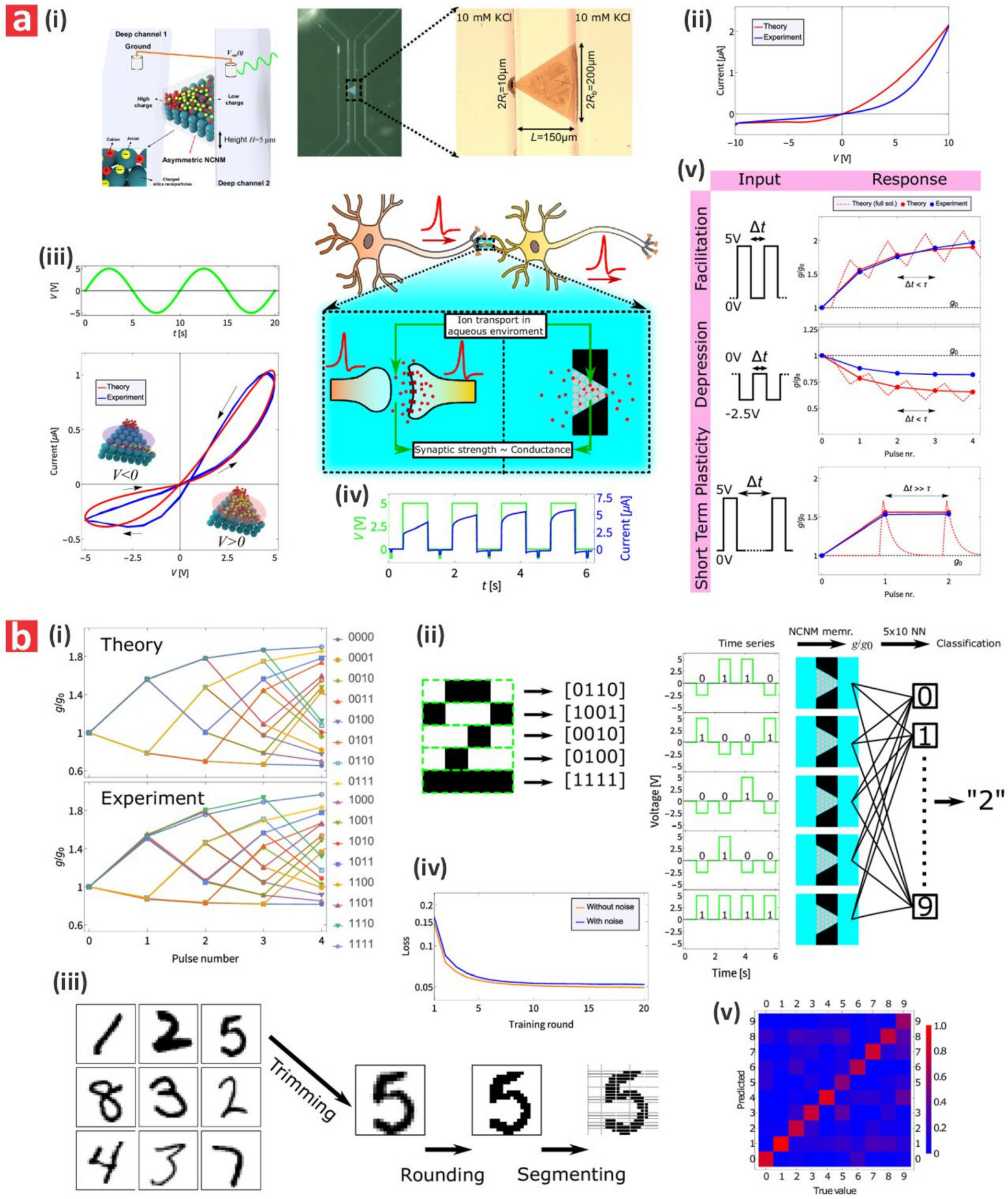

FIG. 12. Fluidic iontronic nanochannels for neuromorphic reservoir computing. (a) Iontronic properties of the proposed fluidic memristor: (i) schematic (left) and photos (right) showing a tapered microchannel with a conducting network of nanochannels embed in a rigid colloidal structure; (ii) steady state I–V profile with ion current rectification; (iii) dynamic I–V profile with ion current hysteresis; (iv) output current response (blue) to applied 5 V write-pulses and –1 V read-pulses (green); and (v) short-term plasticity features exhibited by the device in response to applied voltage pulses of 5 V and –2.5 V. (b) Proof-of-concept demonstration as synaptic element in reservoir computing: (i) the change in device conductance corresponding to 16 bit-strings; (ii) the interpretation of number "2" to 5 bit-strings (left) and subsequent translation to 5 voltage train/conductance values (right); (iii) the conversion of handwritten numbers to 110 bit-strings, involving trimming of pixelated image, rounding of grayscales, and image segmenting; (iv) the loss function during training indicating a negligible effect of noise on accuracy; and (v) the confusion matrix on a test set of 2000 samples depicting an accuracy of 81%. Reprinted (adapted) with permission from Kamsma *et al.*, Prod. Natl. Acad. U. S. A. **121**, e2320242121 (2024). Copyright 2024 Authors; licensed under a Creative Commons Attribution (CC-BY) license.[20]

ion transport across ionic transistors is regulated by a gate voltage.[95,96] An ionic transistor is typically a three-electrode system consisting of a synthetic ion channel, the function of which is to connect the source and drain electrolyte reservoirs, as illustrated in Fig. 13(a). An external bias applied between the electrodes in each reservoir drives the flow of ions across the ion channel that separates the two reservoirs. The behavior of ionic flow across the channel (i.e., selectivity and ionic current) can be controlled by the introduction of a gate voltage. The

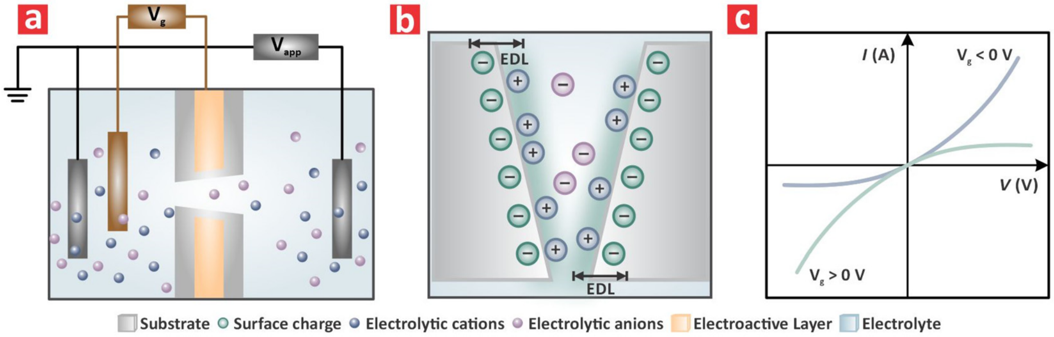

FIG. 13. Fundamental principles of fluidic transistors. (a) A representative setup of a fluidic transistor consisting of a cone-shaped nanochannel, and three terminal electrodes immersed in an electrolyte solution. (b) Illustration of the electrical double layer (EDL) formed on a negatively charged nanochannel wall. (c) Current–voltage (*I*–*V*) profile of a fluidic transistor.

application of a gate voltage results in a change in the surface charge of the ion channel, which attracts counterions but repels co-ions as electrolytic ions flow through the channel. Depending on the selectivity of the ion channels, fluidic transistors can be classified into either p-type or n-type.[95]

The transport of charged species across fluidic transistors is fundamentally governed by the EDL theory. In a fluidic transistor system such as the one shown in Fig. 13(b), a diffuse layer comprising an enrichment of counterions and repulsion of co-ions is formed at the interface between the channel substrate and the electrolyte due to the presence of fixed surface charge density on the channel.[97,98] The electrostatic potential associated with the EDL changes exponentially as the diffuse layer extends from the channel wall to the bulk electrolyte solution. When the Debye length—thickness of EDL—is approximated that of the size of the channel at the nanometric scale, the overlapping between the EDLs at both interfaces of the channel wall and solution leads to the generation of an electrostatic field within the channel. This allows the ions within this region to be controlled independently by electrostatic force.[95,99] The movement of ionic charges across this finite region of the EDL facilitated by applied source and drain biases can be regulated by modulating the surface charge density of the channel through the introduction of a gate voltage.

When no gate voltage is applied, cations and anions flow in opposing direction with a decaying potential to a minimum at the center of the channel. The flow of negatively charged anions can be enhanced while suppressing the flow of positively charged cations by applying a positive gate voltage. In this case, anions are the main charge carriers due to the polarization of the channel wall by a gate voltage > 0 V. Conversely, cations act as major signal carrier as the channel wall is negatively charged by a gate voltage < 0 V that favors the flow cations over that of anions. Hence, the polarity of fluidic transistors can be tuned by the applied gate voltage and the associated ionic flux can be electrically characterized by current–potential profile, as shown in Fig. 13(c).[95] Based on the variation of ionic current over a range of scanning potential at different gate voltages, the ratio of ON state (high ionic conductivity) to OFF state (low ionic conductivity) currents, also known as gating ratio, can be determined to define the gating performance of a fluidic transistor.[100] The EDL theory involved in the ion transport behavior of fluidic transistors can be mathematically represented by Poisson–Boltzmann equation, which describes the electrostatic potential of the surface in terms of the following equation:[100]

$$\nabla^2 \varphi(r) = \frac{-e \sum_i C_i z_i}{\varepsilon \varepsilon_0} = \frac{-e}{\varepsilon \varepsilon_0} \times \sum_i C_{0,i} \exp\left(\frac{-\varphi(r) z_i e}{k_B T}\right) z_i, \quad (3)$$

where C_i and $C_{0,i}$ are concentrations of the i-compound at position r and in the bulk, respectively, k_B is the Boltzmann constant, T is the temperature, e is the electron charge, z_i is the ion valence, ε and ε_0 are the relative permittivities of the medium and vacuum, respectively, and $\psi(r)$ is electrostatic potential. Note that $\psi(r)$ can be expressed by the Debye–Hückel approximation for a low charged planar surface by correlating the electrostatic potential at the surface ψ_0 and Debye–Hückel parameter κ

$$\varphi(r) = \varphi_0 \exp(-\kappa r). \quad (4)$$

Based on the Debye–Hückel approximation and the electroneutrality principle, the surface charge density, σ, of a fluidic transistor can be estimated using Eq. (5) by considering λ_D–characteristic thickness of EDL.[100]

$$\sigma = \frac{\varphi_0 \varepsilon \varepsilon_0}{\lambda_D}. \quad (5)$$

In transistors, the gate electrode acts as a presynaptic input terminal, analogous to an axon, while the drain electrode functions as postsynaptic output terminal, similar to a dendrite. The functionalities of a biological synapse can be mimicked by modulating the channel conductance that functions as a synaptic weight, through the application of voltage pulses to the gate (presynaptic) and drain (postsynaptic) terminals. The performance of a synaptic device, however, depends on various factors, including the device structure, the materials used for the active channel, operational stability, synaptic behaviors, and energy consumption per synaptic event.[101]

B. Materials, architectures, and operations

The iontronic performance of a fluidic transistor is determined by the ion transport behavior across the system, which is critically determined by the properties of ion channels and gate electrodes. Synthetic ion channels in a fluidic transistor system are often in the form of nanopores, nanochannels, and nanotubes composed of polymeric (polyimide and polycarbonate) and inorganic ceramic materials (silica and alumina). They are fabricated by various methods such as lithography, ion beam sculpting, chemical and electrochemical etching, ion track etching, chemical vapor deposition, and self-assembly. These techniques allow the versatile tuning of the geometrical shape, size, and symmetry of synthetic nanochannels.[102–104] Note that some fluidic transistors featuring geometrically asymmetric nanopores and inhomogeneous surface charge distribution exhibit diode-like rectifying behavior.[105–107] To provide the fluidic transistor system with electrical responsiveness for the modulation of ionic current via external voltages, the synthetic ion channels are usually integrated with electrical conductors by sputtering, spin coating, electropolymerization, or electroless deposition.[95,100,104] Based on the type of conducting materials employed as gate electrodes, these fluidic transistors are classified into inorganic, inorganic/organic, and organic fluidic field-effect transistors.[100] For an inorganic fluidic transistor, track-etched polycarbonate and polyester membranes, silica-based nanochannels, and silicon nitride nanopores are modified with a layer of metal or metal oxides (i.e., gold and titanium nitride), the surface charge density of which can be tuned by an externally applied gate potential.[108–116] Upon an applied gate voltage, the alignment of its polarity in the same or opposite direction as the native surface charge of synthetic ion channel results in an increment, neutralization, or reversal of surface charge polarity, which in turn modulates the ionic current.[117] A representative example of inorganic fluidic transistor is provided in Fig. 14(a).[109] Track-etched or alumina membrane-based inorganic/organic fluidic transistors consist of both metal and polymer layers for their respective electrical conductivity and redox properties, as displayed in Fig. 14(b).

Their gating principle is based on the redox transformation of the electroactive polymer and the associated change in its physicochemical properties at the channel entrance surface. The oxidation/reduction of electroactive polymer induced by an applied gate bias leads to a localized variation in its surface charge, volume and hydrophobicity, modulating the resulting ionic current signals.[118–123] In contrast to the other types of transistors, organic transistors are made up of synthetic ion channels functionalized with only organic molecules, i.e., polymers with high electrical conductivity. The ion transport properties of organic transistors are controlled by the net charge variation of the conducting polymer related to its redox states at different gate biases, as shown in Fig. 14(c). The resulting diffuse layer at the polymeric interface exhibits counterions screening, regulating the ionic selectivity of organic transistors.[124,125] In addition to the aforementioned fluidic transistors, two dimensional materials (e.g., graphene oxide, molybdenum disulfide, transition metal carbides, or nitrides) featuring subnanometric channels between the stacking layers within the laminar membrane are also employed in ionic transistors as they exhibit ultrafast ion transport and higher selectivity for better gating effect.[126–129] The gate electrodes in ionic transistors can be wrapped around the nanochannel, located on one side of the nanofluidic membrane or in the middle of a nanopore, which have an impact on the ion concentration polarization in the EDL and its concomitant ionic current.[107,130] The interplay between the design of nanofluidic transistors (i.e., gate electrode, electroactive polymer, and channel geometry) and electrolytes also enables the switching of ion transport behavior among Ohmic, anion-driven, and cation-driven regimes.[126,131]

C. Recent advances in other fluidic computing components for neuromophic applications

By harnessing ions as signal carriers, fluidic field-effect transistors can emulate neuron and synapse functions such as long- and short-term memory, biological oscillations, and action potential-based pulse signals, to achieve neuromorphic computing.[95] Voltage-gated potassium channels in neurons are involved in establishing resting membrane potential and action potential waveform, as well as regulating the release of neurotransmitters, through the closing, opening, and activation of channel states controlled by membrane voltage.[132] Funnel-shaped nanochannels composed of PET modified with 4'-aminobenzo-18-crown-6 (4-AB18C6) were fabricated to mimic these potassium channels. The underlying working principle of this system was based on the release of bound potassium (K^+) ions from the 4-AB18C6 functional layer upon the application of an external voltage. The gating ability of 4-AB18C6-functionalized nanochannels was established by a decrease in gating ratios from 1.0 to 0.25 based on the ratio of ionic currents before and after addition of K^+ at a gate potential of $\pm$ 1.4 V. The voltage-responsive characteristic of the K^+-activated gating nanochannel was demonstrated by the varying ionic currents at different applied bias from the change in surface charge properties and wettability induced by the release of K^+ from the 4-AB18C6 layer. This led to a higher ionic current as the nanochannels transit from closed to opened state.[133]

The potential neuromorphic application of bioinspired carbon nanotube-based nanofluidic ionic transistors was demonstrated through the construction of ionic logic circuits. Asymmetric (ACNT) and symmetric (CNT) carbon nanotubes were used to construct unipolar and ambipolar nanofluidic ionic transistors, respectively, with the integration of anodic aluminum oxide as a dielectric layer. The ion transport across CNT was governed by the applied gate potential: (i) at positive potential, the negative charges on CNT was neutralized with a reduction in ion carrier concentration and hence OFF state; and (ii) negative potential promotes the formation of more negative charges on CNT with an increase in ion flow and hence ON state. The gating ratios of ACNT as unipolar ionic transistor and CNT-based ambipolar ionic transistor were determined to be 10^4 and 479 at a gate potential of 1 V, respectively. Using CNT-based nanofluidic ionic transistors, a logic circuit system comprising NOT, NAND, and NOR gates was constructed, where their output logic states were modulated by external gate voltages.[134]

Similar ionic gate circuits, i.e., NOT, NAND, and NOR, for neuromorphic signal processing were also achieved by a two-dimensional nanofluidic ionic transistor based on a MXene membrane (Fig. 15). The nanochannels created by the interlayer spacing of the multilayered MXene membrane featured high surface charges from C–O and C = O moieties, enabling the switching between ON and OFF states by modulating the unilateral gate voltage from negative to positive values. A gating ratio as high as 2000 was reached at gate potentials of $\pm$1 V in 1 mM KCl electrolyte. The transitional conductivity between n-type and p-type was demonstrated through the manipulation of the bias voltage vector, establishing the bipolar characteristics of MXene-based ionic transistors. This bipolar state was altered to unipolar when the degree of structural asymmetric increased with the thickness of MXene membrane. As a proof-of-concept, a PET/MXene asymmetric composite membrane-based ionic transistor with unipolar properties, characterized by a switchable ON/OFF state at negative bias but only OFF state at positive bias, was used to realize the basic NOT gate with the integration of a resistor. It produced an output signal of 0.5 V at the OFF state when an input signal of 0 V was introduced. Conversely, the output signal dropped to 0 V when the ionic transistor in the NOT

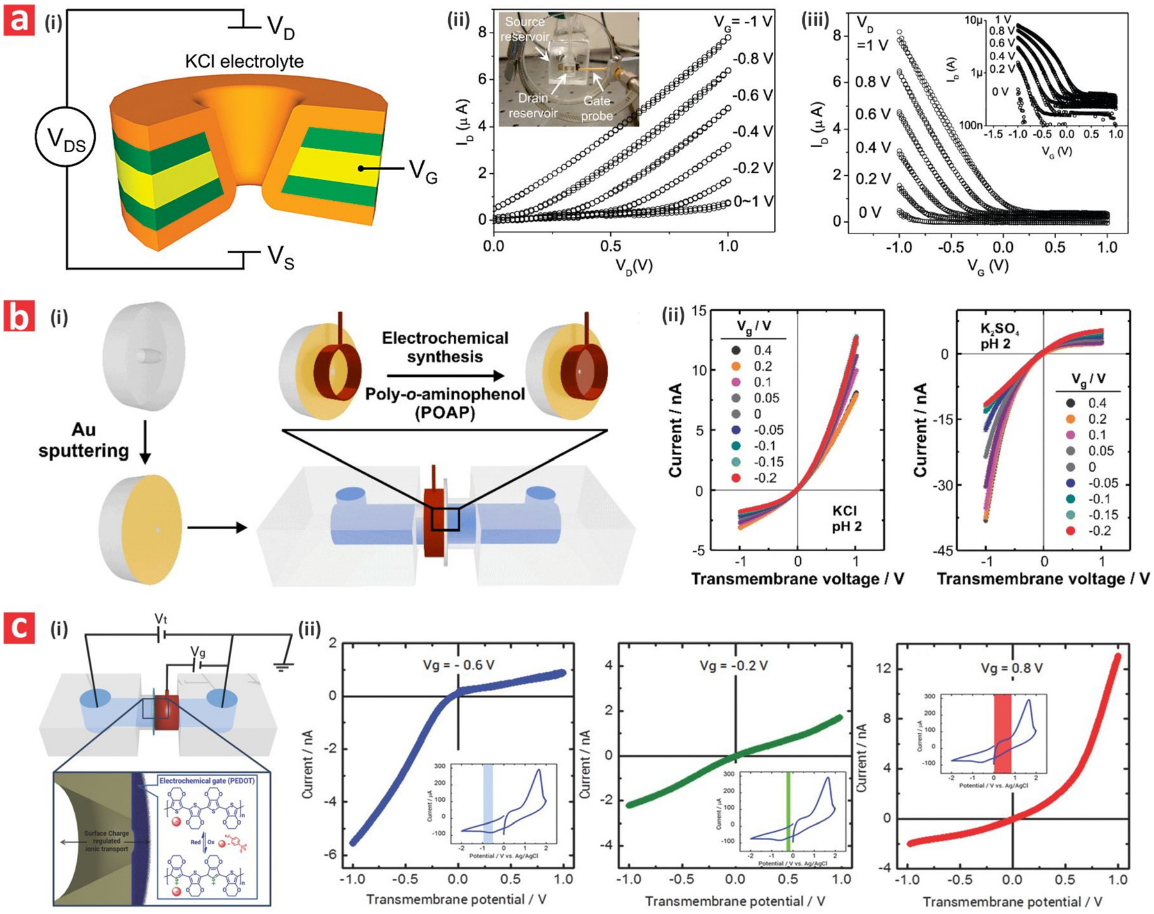

FIG. 14. Representative examples of fluidic transistors of different materials and architectures. (a) Inorganic fluidic field-effect transistors: (i) silicon nitride-based nanopore (green) device surrounded by titanium dioxide gate dielectric (orange) and titanium nitride gate electrode (yellow); *I–V* responses under different applied gate voltages ranged from (ii) –1 to 0 V; and (iii) 0 to 1 V. Reprinted (adapted) with permission from Nam *et al.*, Nano Lett. **9**, 2044–2048 (2009). Copyright 2009 American Chemical Society.[109] (b) Inorganic/organic fluidic flied-effect transistors: (i) poly(ethylene terephthalate (PET)-based nanochannel modified with layers of gold and poly-*ortho*-aminophenol; (ii) characteristic *I–V* profiles as a function of gate voltages in potassium chloride (KCl–left) and potassium sulfate (K_2SO_4–right) solutions. Reprinted (adapted) with permission from Laucirica *et al.*, Nanoscale **15**, 1782–1793 (2023). Copyright 2023 Royal Society of Chemistry.[122] (c) Organic fluidic field-effect transistors: (i) PET-based nanochannel modified with a layer of PEDOT conductive polymer and their (ii) *I–V* profiles in response to gate voltages of –0.6 V (left), –0.2 V (middle), and 0.8 V (right). Reprinted (adapted) with permission from Pérez-Mitta *et al.*, Adv. Mater. **29**, 1700972 (2017). Copyright 2017 John Wiley and Sons.[124]

gate was at its ON state under an input signal of 1 V. Complex NAND and NOR logic gates were further realized by integrating MXene-based ionic transistors with diodes and resistors, which could be applied to the building of ionic circuits with higher complexity for brain-like computing.[135]

The synaptic plasticity of neuronal synapse is measured by the change in the strength of synaptic junctions, i.e., synaptic weight, with electrical action potential spikes, defining the efficiency of information processing between neurons. To realize neural plasticity, synaptic iontronic devices use directional movement of ions and conductance change under pulse signals to simulate spike-induced synaptic weight change.[36] Based on this concept, an artificial synapse based on inorganic/organic transistor was realized and its synaptic plasticity was selectively modulated by the enzymatic reaction between glucose and glucose oxidase (GOx). In this fluidic transistor (Fig. 16), poly (3,4-ethylenedioxythiophene):poly(styrene sulfonate) (PEDOT:PSS) was used as postsynaptic channel and gold/chromium (Au/Cr) as gate electrodes. These gate electrodes were decorated with a mixture of GOx, single walled carbon nanotubes and platinum nanoparticles to provide specific recognition toward glucose. The conductance (synaptic weight) of PEDOT:PSS postsynaptic channels was regulated by the transport of injected ions from the aqueous electrolyte through the application of gate potentials. Cations introduced into the channel under positive gating voltage filled in the holes in the PEDOT backbones and caused a decrease in channel conductance, inferring an inhibitory postsynaptic current (depression behaviors). Conversely, an excitatory postsynaptic current (potentiation behaviors) was triggered by negative gate voltage pulses. Short-term modulation of channel conductance was attained at a single positive voltage pulse (0.3 V for 2 s) in the absence of glucose in phosphate-buffered saline (PBS)

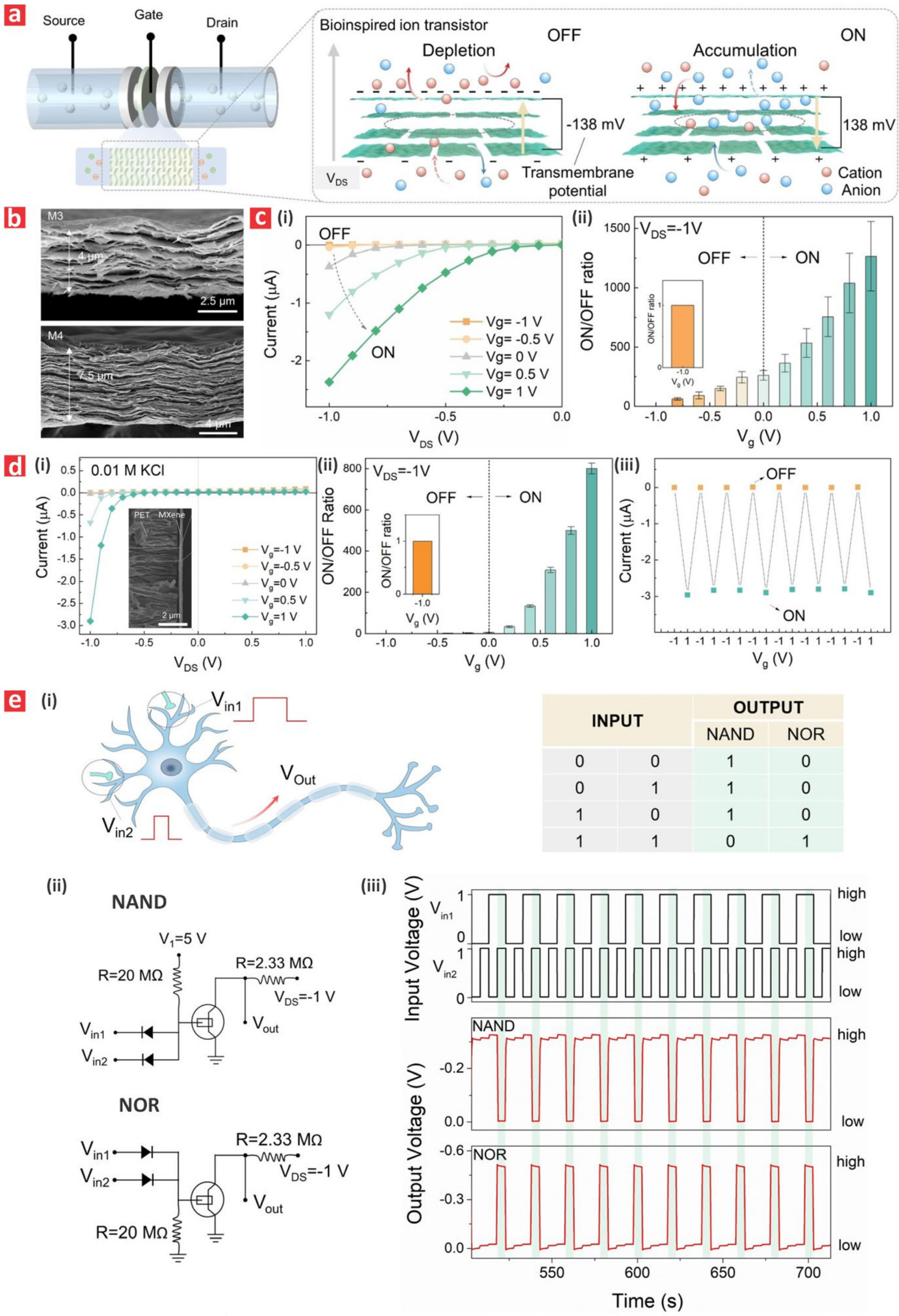

FIG. 15. MXene-based fluidic transistor for neuromorphic signal processing. (a) Schematic of symmetric ionic transistor composed of two-dimensional MXene membrane and its OFF and ON state under a transmembrane potential of ± 138 mV. (b) SEM cross-sectional view of MXene membranes with thicknesses of 4 and 7.5 μm. (c) Electrical characterization of symmetric MXene-based ionic transistor in terms of (i) *I–V* curves at gate voltages in the range of –1 to 1 V and (ii) the corresponding gating ratio. (d) Electrical characteristics of asymmetric MXene-based ionic transistor modified further with PET determined by (i) *I–V* profiles acquired at different gate voltages (–1 to 1 V); (ii) their respective gating ratios; and (iii) gating performance and stability under alternating –1 and 1 V gate voltage. (e) Neuromorphic signal processing using logic gates with MXene/PET composite ionic transistor: (i) illustration of signal procession of a nerve cell and the truth table of basic logic "NAND" and "NOR" gate; (ii) equivalent circuit of ionic "NAND" and "NOR" gates with the connection to diodes and resistors; (iii) experimental signal integration performance of ionic logic gates. Reprinted (adapted) with permission from Mei *et al.*, Angew. Chem. Int. Ed. **63**, e20241477 (2024). Copyright 2024 John Wiley and Sons.[135]

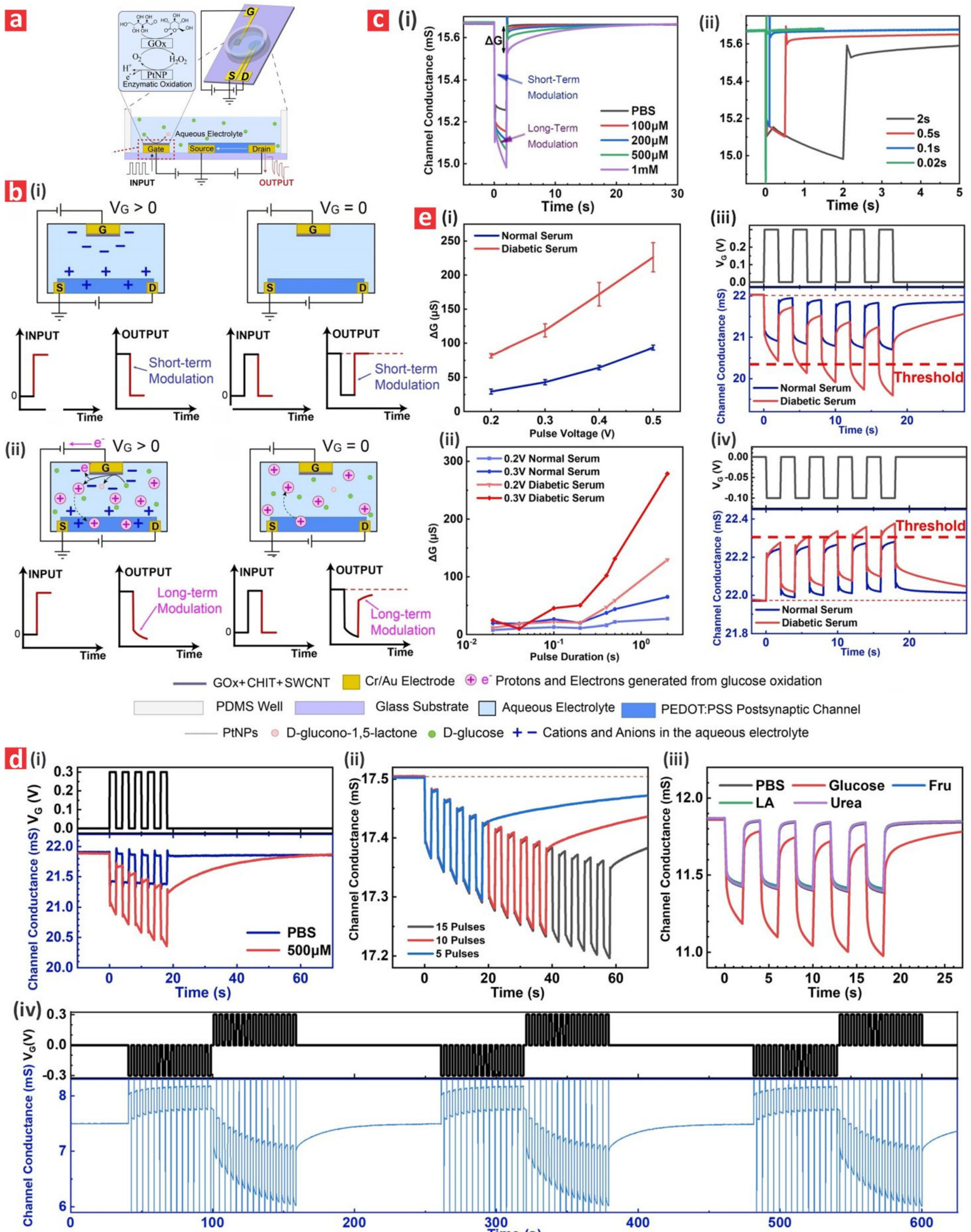

FIG. 16. An artificial synapse based on ionic transistor. (a) The construction of artificial synaptic device based on PEDOT:PSS and Au/Cr gate electrodes modified with Pt nanoparticles and glucose oxidase; (b) Schematics of the working principle of the proposed artifice synapse based on the conductance change induced by the oxidation of glucose: (i) short-term modulation of device conductance by V_{app}; (ii) long-term modulation of device conductance by glucose oxidation. (c) Electrochemical characterization of the artificial synapse showing (i) short-term and long-term modulation of conductance by a single voltage pulse in PBS solutions with different glucose concentrations; (ii) the synaptic performance at different pulse duration in PBS solution. (d) Memory and learning ability of the synaptic device at various conditions: (i) PBS solution with 0 and 500 μM of glucose; (ii) different numbers of successive pulses (5, 10, and 15); (iii) PBS solution containing different biomolecules of 500 μM (fructose, urea, and lactic acid); and (iv) alternating positive and negative pulses (20 cycles) for long-term potentiation and depression. (e) Synaptic behavior of the proposed device in human blood serum: change in device conductance as a function of (i) pulse amplitude and (ii) pulse duration; (iii) cumulative de-doping and memory effect in normal and diabetic serum under positive successive pulses; and (iv) cumulative doping and memory effect in normal and diabetic serum under negative successive pulses. Reprinted (adapted) with permission from Xu *et al.*, Angew. Chem. Int. Ed. **62**, e202302723 (2023). Copyright 2023 John Wiley and Sons.[136]

electrolyte, where the conductance returned to its initial state immediately when the voltage pulse was removed. However, the induced conductance change exhibited both long- and short-term modulation under the same voltage pulse with the presence of glucose in the PBS electrolyte. A conductance change of 275 ± 19 μS was observed when 1 mM of glucose was added to the PBS, which attained for > 25 s after the removal of the voltage pulse. This long memory retention (depression behavior) was attributed to the irreversible oxidation of glucose and hydrogen peroxide by-products. The selectivity of the proposed transistor was demonstrated by the absence of long-term conditioning of channel conductance in the presence of urea, lactic acid, and fructose, emulating the specificity of postsynaptic membranes. To mimic memorizing and learning behavior in biological nerve systems, 5 successive positive gate potential pulses were applied to the PEDOT:PSS transistor in glucose-containing PBS electrolyte. This resulted in a cumulative de-doping of the PEDOT:PSS channel, which gave rise to memory and retention effects that could be further enhanced by increasing the voltage pulse series. The proposed transistor also showed enhanced synaptic behavior in blood serum at a higher glucose concentration (i.e., diabetic serum), implying potential *in vivo* applications as artificial neurons.[136]

Sabbargh *et al.* have successfully assembled iontronic circuits by integrating multiple bipolar polyelectrolyte (pDADMAC and pAMPSA) diodes as ionic logic gates. Two different individual diode-based logic gates (DLG), i.e., OR DLG and AND DLG were constructed in the form of microfluidic chips, where the former has the conductive direction of the diodes faced inward to the center of circuit and outward for the latter. Note that the operating condition of logic gate circuit was optimized based on the characteristic of single polyelectrolyte diode in terms of rectification ratio, applied voltages, resistor–capacitor time constant. OR DLG produced a high potential when at least one of its inputs was of high level whereas the output of AND DLG was of low logic level depending on how and which input was low. They also demonstrated logic computation by integrating multiple iontronic DLG in a parallel and series. The parallel circuit consists of two OR DLG with three inputs and two outputs whereas the series circuit has the output of AND DLG connected to one of the two inputs of OR DLG. They were able to maintain the correct output logic level for all 2^3 possible input sequences. The performance of two-stage cascade with three DLGs of different combinations were also investigate, which showed reliable output results. However, the cascading of four OR DLG in series resulted in false logic readout.[137]

They have also used a similar polyelectrolyte-based system, but with the integration of fluorescence cationic and anionic dye molecules, to perform Boolean operation of an ionic OR logic gate (Fig. 17). Low (0) and high (1) logic inputs were realized by applying 0 and 1 V, respectively, where the output readouts have their logic levels based on measure potential or fluorescence intensity. Each input of the OR logic gate was connected through a diode to an interconnecting polyelectrolyte-filled readout spot. The addition of fluorescence dye into one or both input, logic level 1, resulted in flow of current through the forward-biased diodes and a voltage decrease was induced (logic output 1). These studies have provided the fundamentals to enable the realization of more complex and advanced ionic computing functions.[138]

Throughout the review we have emphasized that the memristive property of fluidic nanochannels, composed of rectification and hysteresis, enables the functionalities of synapses, with more or less volatile qualities according to the relaxation time τ that determines the retention times. The other essential component for biology-like computation is the neuron. In a neuromorphic system, a neuron functions as a node that integrates incoming signals from other connected neurons. Natural neurons communicate through spiking signals, which are brief electrical impulses called action potentials. These signals originate from voltage-gated ion channels located in the neuron's membrane. These channels regulate the flow of ions (such as sodium, potassium, and calcium) in and out of the neuron, which generates and propagates electrical activity. The spiking signals, which mimic biological synaptic inputs, can be excitatory (increasing the likelihood of activation) or inhibitory (decreasing it). The neuron accumulates these inputs over time, similar to how a biological neuron integrates synaptic potentials. Once the combined input reaches a certain threshold, the neuron fires an output signal (a spike), which is then transmitted to downstream neurons. This process enables neuromorphic systems to efficiently perform computations in a brain-inspired manner, such as pattern recognition and learning.

The main reference for the operation of natural neurons is the Hodgkin–Huxley (HH) model that mathematically describes the process of spiking using four differential equations.[57,139,140] This model captures the temporal dynamics of protein ion channels by accounting for:

1. The neuron's membrane potential (voltage across the membrane).
2. The gating variables that control the opening and closing of ion channels.
3. The ionic currents carried by sodium ions (Na^+), potassium ions (K^+), and a small leak current.
4. The changes in conductance over time due to these ion flows.

By solving these equations, the HH model accurately replicates how neurons generate and transmit spikes, making it a fundamental framework for understanding neural excitability and neuromorphic computing.

Clearly, the fluidic nanochannels form an ideal framework to reproduce the functionalities of natural neurons to form biologically faithful spiking neural networks, since both are based on ionic properties through narrow channels. However, memristive properties described before are not sufficient to form spiking. To obtain a self-sustained oscillation, mimicking the repetitive action potential, under a constant stimulus, the fluidic device needs to have the property of a bifurcation.[141,142] It means that the system contains a sudden dynamical change under a small variation of a parameter. In neuronal dynamics and electrochemical systems this feature requires that the system contains a negative resistance that destabilizes the system to form the oscillatory behavior.[143] Several results have been presented of potential neuron elements based on fluidic nanochannels, using two different strategies:

i. Creating a spiking system based on two equations. This method starts from Eqs. (1) and (2) and introduces a negative resistance feature.[144] A full characterization of the bifurcation properties indicates the plausible regimes of parameters of the nanopore.[145] The result is an oscillatory voltage as in the traditional electrochemical oscillation systems.[146] The advantage of this method is that it is formed with a single pore.

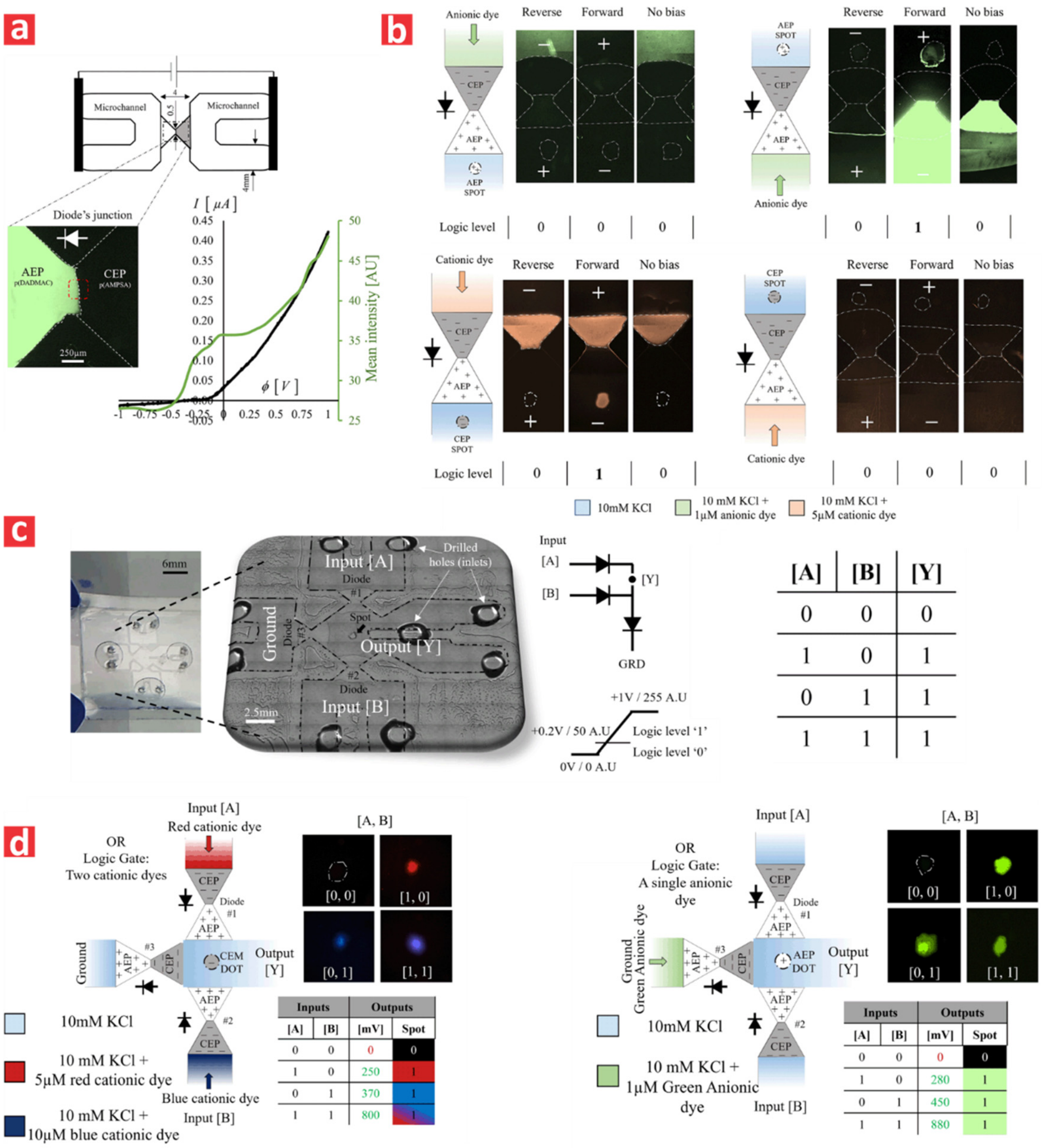

FIG. 17. Integration of iontronic logic gates using polyelectrolyte-based diodes. (a) A microfluidic diode consisting of two microchannels joined by a narrow junction interfacing anion- and cation-exchange polyelectrolytes, characterized by hysteresis loops in *I–V* curve. (b) Single bipolar diode gating for anionic (1 μM) and cationic (5 μM) dye with anion- and cation exchange polyelectrolyte spot, respectively. The fluorescence intensities measured on the spot were translated into logic level of 0 and 1 corresponding to different bias (reverse: –1 V, forward: 1 V, and no bias: 0 V). (c) Microfluidic OR logic gate using diode with the truth table of OR gate. (d) Schematic showing three diodes-integrated OR logic gate with two inputs of 0 (low) and 1 V (high), and an output readout region. The introduction of cationic (left) and anionic (right) fluorescence dye into the system at different input induced different fluorescence effect at the readout spots, which were summarized in the truth tables. Reprinted (adapted) with permission from Sabbagh *et al.*, Faraday Discuss. **246**, 141 (2023). Copyright 2023 Authors; licensed under a Creative Commons Attribution (CC BY) license.[138]

ii. Reproducing the full HH model.[24,29] This method requires to combine several nanochannels to mimic the separate action of potassium and sodium channels. Again, this method necessarily requires a negative resistance effect (which in HH model is in the sodium channel). This method is more complex than (i), but it can produce more elaborated spiking and bursting neuronal patterns with advanced biological functionalities.

To our knowledge, a practical realization of these neuronal systems has not been reported yet.

IV. OUTLOOK AND CONCLUSIONS

Fluidic iontronics, inspired by signal transmission mechanism of biological synapses, has emerged as a promising approach to complement current solid-state computing technology, advancing the field of neuromorphic computing and extending the field of AI to systems based on brain mechanisms. The adaptation of ions as signal carriers in fluidic iontronics enables a more energy-efficient, stable, flexible mean of realizing synaptic functionalities and delivering new computing capabilities based on the diversity of ions and their distinct chemical properties. Through the regulation of ionic behavior under confinement, fluidic iontronic architectures such as ionic transistors and memristors have achieved bioinspired logic functions and brain-like neural signals. Nonetheless, the existence of a wide variety of ions with their own unique characteristics poses significant challenges to precise and effective regulation of ions as well as accurate information reading and processing. Further investigation into the fundamental mechanisms associated with ion diffusion, equilibria, and transport that govern the ionic memory and logic operation in these fluidic devices is required to gain a deeper understanding of the correlation between device architecture (i.e., surface charge and channel geometry) and system performance (i.e., gating ratio, memory timescale, and hysteresis magnitude). This would enhance the ability of these fluidic devices to perform higher-complexity neuromorphic functions while solving challenges related to scalability and interconnectivity. The capability and robustness of synaptic iontronic devices could also be expanded by (i) coupling with electronics to address some of their inherent limitations correlated with ion mobility and size; (ii) using multiple types of ionic carriers to develop fluidic neuromorphic devices with ion-specific readouts for many different possible states, instead of simply ON or OFF states; (iii) adopting a biocompatible or implantable device structure for potential autonomous control by biological systems and direct communication with biological signal and regulatory pathways; (iv) large-scale integration of fluidic transistor and memristor systems into a compact interconnected array network for broader parallel operations of complex neuromorphic computing tasks; and (v) implementing artificial neural network models such as grow-when-required and convolutional neural networks for the incorporation of dynamic and adaptive features in fluidic brain-like computing. While neuroplasticity such as Hebbian learning has been demonstrated by fluidic synaptic systems, there is still more to explore and optimize in terms of physics, chemistry, electronics, and materials science. Advanced lithography processes and flow engineering could be adopted to develop nanofluidic electronics, by implementing fluidic capillaries, spring probe-based electrical contacts, and extended gate configuration in very-large-scale integration (VLSI) processes. The seamless integration of theses fluidic elements with conventional electronics could be facilitated by using CMOS-compatible materials. By training the network on-chip through learning, each component in the fluidic systems could be tuned by taking the characteristics of each elements into consideration to leverage device variability. The implementation of algorithm could also compensate device variations. These advances will be needed to achieve precise recognition of input pulses with temporal proximity and realize more complex neuronal functions. Furthermore, the micro- and nanofabrication techniques used to produce fluidic systems are well-established and industrial scalable, making large-scale production possible. Although the ion–surface interaction kinetics in fluidic neuromorphic systems might impact their long-term stability and reliability, lab-scale fluidic systems have demonstrated promising performance stability and device reusability when clean and store appropriately, suggesting their potential long-term practical deployment. By choosing the appropriate materials to fabricate fluidic neuromorphic systems not only the stability and durability could be improved but also help to reduce production cost. Nonetheless, it is undeniable that artificial channel-based fluidic systems have the potential to deliver synaptic functionalities for neuromorphic computing with energy- and performance-efficiency comparable to that of biological neurons, paving the way for next-generation computing devices in this era of big data.

ACKNOWLEDGMENTS

Authors would like to acknowledge and pay their respects to the Kaurna–Adelaide people, the Traditional Custodians of the land on which the work was performed. A.S. and A.D.A. thank the support provided by the Australian Research Council through the Grant No. DP220102857, the School of Chemical Engineering, the University of Adelaide, the Institute for Photonics and Advanced Sensing (IPAS). J.B. thanks the support provided by European Research Council via Horizon Europe Advanced Grant, grant agreement No. 101097688 ("PeroSpiker"). C.S.L. thanks the support provided by the University of Adelaide and IPAS through her Future Making Fellowship.

AUTHOR DECLARATIONS

Conflict of Interest

The authors have no conflicts to disclose.

Author Contributions

Cheryl Suwen Law: Conceptualization (equal); Data curation (lead); Funding acquisition (equal); Investigation (lead); Project administration (lead); Resources (lead); Writing – original draft (lead); Writing – review & editing (equal). **Juan Wang:** Conceptualization (equal); Data curation (lead); Formal analysis (equal); Funding acquisition (equal); Investigation (lead); Writing – original draft (lead); Writing – review & editing (equal). **Kornelius Nielsch:** Formal analysis (equal); Funding acquisition (equal); Writing – review & editing (equal). **Andrew D. Abell:** Funding acquisition (equal); Writing – review & editing (equal). **Juan Bisquert:** Formal analysis (equal); Funding acquisition (equal); Writing – review & editing (equal). **Abel Santos:** Conceptualization (equal); Formal analysis (equal); Funding acquisition (lead); Investigation (equal); Project administration (lead); Resources (lead); Writing – review & editing (equal).

DATA AVAILABILITY

The data that support the findings of this study are available from the corresponding authors upon reasonable request.

REFERENCES

[1] J. G. Carrasco Ramírez and M. Islam, "Utilizing artificial intelligence in real-world applications," J. Artif. Intell. Gen. Sci. **2**, 14 (2024).

[2]A. Goel, A. K. Goel, and A. Kumar, "The role of artificial neural network and machine learning in utilizing spatial information," Spat. Inf. Res. **31**, 275 (2023).
[3]I. H. Sarker, "Machine learning: Algorithms, real-world applications and research directions," SN Comput. Sci. **2**, 60 (2021).
[4]V. K. Sangwan and M. C. Hersam, "Neuromorphic nanoelectronic materials," Nat. Nanotechnol. **15**, 517 (2020).
[5]D. Ivanov, A. Chezhegov, and D. Larionov, "Neuromorphic artificial intelligence systems," Front. Neurosci. **16**, 959626 (2022).
[6]M. A. Zidan, J. P. Strachan, and W. D. Lu, "The future of electronics based on memristive systems," Nat. Electron. **1**, 22 (2018).
[7]D. Marković, A. Mizrahi, D. Querlioz, and J. Grollier, "Physics for neuromorphic computing," Nat. Rev. Phys. **2**, 499 (2020).
[8]B. Sun, T. Guo, G. Zhou, S. Ranjan, Y. Jiao, L. Wei, Y. N. Zhou, and Y. A. Wu, "Synaptic devices based neuromorphic computing applications in artificial intelligence," Mater. Today Phys. **18**, 100393 (2021).
[9]C. D. James, J. B. Aimone, N. E. Miner, C. M. Vineyard, F. H. Rothganger, K. D. Carlson, S. A. Mulder, T. J. Draelos, A. Faust, M. J. Marinella *et al.*, "A historical survey of algorithms and hardware architectures for neural-inspired and neuromorphic computing applications," Biol. Inspired Cogn. Archit. **19**, 49 (2017).
[10]N. Rathi, I. Chakraborty, A. Kosta, A. Sengupta, A. Ankit, P. Panda, and K. Roy, "Exploring neuromorphic computing based on spiking neural networks: Algorithms to hardware," ACM Comput. Surv. **55**, 1 (2023).
[11]D. S. Modha, F. Akopyan, A. Andreopoulos, R. Appuswamy, J. V. Arthur, A. S. Cassidy, P. Datta, M. V. DeBole, S. K. Esser, C. O. Otero *et al.*, "Neural inference at the frontier of energy, space, and time," Science **382**, 329 (2023).
[12]F. Akopyan, J. Sawada, A. Cassidy, R. Alvarez-Icaza, J. Arthur, P. Merolla, N. Imam, Y. Nakamura, P. Datta, G. J. Nam *et al.*, "Truenorth: Design and tool flow of a 65 mW 1 million neuron programmable neurosynaptic chip," IEEE Trans. Comput.-Aided Des. Integr. Circuits Syst. **34**, 1537 (2015).
[13]H. Bos and D. Muir, "Sub-mW neuromorphic SNN audio processing applications with rockpool and xylo," in *Embedded Artificial Intelligence* (River Publishers, 2023).
[14]S. B. Shrestha, J. Timcheck, P. Frady, L. Campos-Macias, and M. Davies, "Efficient video and audio processing with Loihi 2," in *ICASSP 2024 - 2024 IEEE International Conference on Acoustics, Speech and Signal Processing (ICASSP)* (IEEE, 2024).
[15]O. Richter, Y. Xing, M. De Marchi, C. Nielsen, M. Katsimpris, R. Cattaneo, Y. Ren, Q. Liu, S. Sheik, T. Demirci *et al.*, "Speck: A smart event-based vision sensor with a low latency 327K neuron convolutional neuronal network processing pipeline " arXiv:2304.06793v2 (2023).
[16]B. J. Shastri, A. N. Tait, T. Ferreira de Lima, W. H. Pernice, H. Bhaskaran, C. D. Wright, and P. R. Prucnal, "Photonics for artificial intelligence and neuromorphic computing," Nat. Photonics **15**, 102 (2021).
[17]Y. Wang, L. Yin, W. Huang, Y. Li, S. Huang, Y. Zhu, D. Yang, and X. Pi, "Optoelectronic synaptic devices for neuromorphic computing," Adv. Intell. Syst. **3**, 2000099 (2021).
[18]A. Noy and S. B. Darling, "Nanofluidic computing makes a splash," Science **379**, 143 (2023).
[19]R. Li, Y. Gong, H. Huang, Y. Zhou, S. Mao, Z. Wei, and Z Zhang, "Photonics for neuromorphic computing: Fundamentals, devices, and opportunities," Adv. Mater. **37**, 2312825 (2025).
[20]T. M. Kamsma, J. Kim, K. Kim, W. Q. Boon, C. Spitoni, J. Park, and R. van Roij, "Brain-inspired computing with fluidic iontronic nanochannels," Proc. Natl. Acad. Sci. U. S. A. **121**, e2320242121 (2024).
[21]T. Xiong, W. Li, P. Yu, and L. Mao, "Fluidic memristor: Bringing chemistry to neuromorphic devices," Innovation **4**, 100435 (2023).
[22]H. Chun and T. D. Chung, "Iontronics," Annu. Rev. Anal. Chem. **8**, 441 (2015).
[23]L. Yu, X. Li, C. Luo, Z. Lei, Y. Wang, Y. Hou, M. Wang, and X. Hou, "Bioinspired nanofluidic iontronics for brain-like computing," Nano Res. **17**, 503 (2024).
[24]T. M. Kamsma, W. Q. Boon, T. Ter Rele, C. Spitoni, and R. Van Roij, "Iontronic neuromorphic signaling with conical microfluidic memristors," Phys. Rev. Lett. **130**, 268401 (2023).
[25]Y. He, M. Tsutsui, Y. Zhou, and X. S. Miao, "Solid-state nanopore systems: From materials to applications," NPG Asia Mater. **13**, 48 (2021).
[26]D. Wang, W. Brown, Y. Li, M. Kvetny, J. Liu, and G. Wang, "Hysteresis charges in the dynamic enrichment and depletion of ions in single conical nanopores," ChemElectroChem **5**, 3089 (2018).
[27]T. Xiong, C. Li, X. He, B. Xie, J. Zong, Y. Jiang, W. Ma, F. Wu, J. Fei, P. Yu *et al.*, "Neuromorphic functions with a polyelectrolyte-confined fluidic memristor," Science **379**, 156 (2023).
[28]P. Zhang, M. Xia, F. Zhuge, Y. Zhou, Z. Wang, B. Dong, Y. Fu, K. Yang, Y. Li, Y. He *et al.*, "Nanochannel-based transport in an interfacial memristor can emulate the analog weight modulation of synapses," Nano Lett. **19**, 4279 (2019).
[29]P. Robin, N. Kavokine, and L. Bocquet, "Modeling of emergent memory and voltage spiking in ionic transport through angstrom-scale slits," Science **373**, 687 (2021).
[30]J. S. Najem, G. J. Taylor, R. J. Weiss, M. S. Hasan, G. Rose, C. D. Schuman, A. Belianinov, C. P. Collier, and S. A. Sarles, "Memristive ion channel-doped biomembranes as synaptic mimics," ACS Nano **12**, 4702 (2018).
[31]P. Li, J. Liu, J. H. Yuan, Y. Guo, S. Wang, P. Zhang, and W. Wang, "Artificial funnel nanochannel device emulates synaptic behavior," Nano Lett. **24**, 6192 (2024).
[32]Y. Hou, Y. Ling, Y. Wang, M. Wang, Y. Chen, X. Li, and X. Hou, "Learning from the brain: Bioinspired nanofluidics," J. Phys. Chem. Lett. **14**, 2891 (2023).
[33]Y. Huang, F. Kiani, F. Ye, and Q. Xia, "From memristive devices to neuromorphic system," Appl. Phys. Lett. **122**, 110501 (2023).
[34]J. J. Yang, D. B. Strukov, and D. R. Stewart, "Memristive devices for computing," Nat. Nanotechnol. **8**, 13 (2013).
[35]H. Chen, H. Li, T. Ma, S. Han, and Q. Zhao, "Biological function simulation in neuromorphic devices: From synapse and neuron to behavior," Sci. Technol. Adv. Mater. **24**, 2183712 (2023).
[36]C. Li, T. Xiong, P. Yu, J. Fei, and L. Mao, "Synaptic iontronic devices for brain-mimicking functions: Fundamentals and applications," ACS Appl. Bio Mater. **4**, 71 (2021).
[37]Y. Li, D. Wang, M. M. Kvetny, W. Brown, J. Liu, and G. Wang, "History-dependent ion transport through conical nanopipettes and the implications in energy conversion dynamics at nanoscale interfaces," Chem. Sci. **6**, 588 (2015).
[38]S.-Y. Kim, H. Zhang, G. Rivera-Sierra, R. Fenollosa, J. Rubio-Magnieto, and J. Bisquert, "Introduction to neuromorphic functions of memristors: The inductive nature of synapse potentiation," J. Appl. Phys. **137**, 111101 (2025).
[39]D. Wang, M. Kvetny, J. Liu, W. Brown, Y. Li, and G. Wang, "Transmembrane potential across single conical nanopores and resulting memristive and memcapacitive ion transport," J. Am. Chem. Soc. **134**, 3651 (2012).
[40]W. Brown, M. Kvetny, R. Yang, and G. Wang, "Selective ion enrichment and charge storage through transport hysteresis in conical nanopipettes," J. Phys. Chem. C **126**, 10872 (2022).
[41]J. Bisquert, "Hysteresis, rectification, and relaxation times of nanofluidic pores for neuromorphic circuit applications," Adv. Phys. Res. **3**, 2400029 (2024).
[42]J. Cervera, S. Portillo, P. Ramirez, and S. Mafe, "Modeling of memory effects in nanofluidic diodes," Phys. Fluids **36**, 047129 (2024).
[43]A. Bou, C. Gonzales, P. P. Boix, Y. Vaynzof, A. Guerrero, and J. Bisquert, "Kinetics of volatile and nonvolatile halide perovskite devices: The conductance-activated quasi-linear memristor (CALM) Model," J. Phys. Chem. Lett. **16**, 69 (2025).
[44]J. J. Perez-Grau, P. Ramirez, V. Garcia-Morales, J. Cervera, S. Nasir, M. Ali, W. Ensinger, and S. Mafe, "Fluoride-induced negative differential resistance in nanopores: Experimental and theoretical characterization," ACS Appl. Mater. Interfaces **13**, 54447 (2021).
[45]G. Laucirica, M. E. Toimil-Molares, W. A. Marmisollé, and O. Azzaroni, "Unlocking nanoprecipitation: A pathway to high reversibility in nanofluidic memristors," ACS Appl. Mater. Interfaces **16**, 58818 (2024).
[46]I. W. Leong, M. Tsutsui, S. Murayama, T. Hayashida, Y. He, and M. Taniguchi, "Quasi-stable salt gradient and resistive switching in solid-state nanopores," ACS Appl. Mater. Interfaces **12**, 52175 (2020).
[47]T. Ahmed, S. Walia, E. L. H. Mayes, R. Ramanathan, V. Bansal, M. Bhaskaran, S. Sriram, and O. Kavehei, "Time and rate dependent synaptic learning in neuro-mimicking resistive memories," Sci. Rep. **9**, 15404 (2019).

[48]C. Weilenmann, A. N. Ziogas, T. Zellweger, K. Portner, M. Mladenović, M. Kaniselvan, T. Moraitis, M. Luisier, and A. Emboras, "Single neuromorphic memristor closely emulates multiple synaptic mechanisms for energy efficient neural networks," Nat. Commun. **15**, 6898 (2024).
[49]J. P. Pfister and W. Gerstner, "Triplets of spikes in a model of spike timing-dependent plasticity," J. Neurosci. **26**, 9673 (2006).
[50]J. Bisquert, J. B. Roldán, and E. Miranda, "Hysteresis in memristors produces conduction inductance and conduction capacitance effects," Phys. Chem. Chem. Phys. **26**, 13804 (2024).
[51]J. Bisquert, "Inductive and capacitive hysteresis of current-voltage curves: Unified structural dynamics in solar energy devices, memristors, ionic transistors and bioelectronics," PRX Energy **3**, 011001 (2024).
[52]P. Ramirez, J. Cervera, S. Nasir, M. Ali, W. Ensinger, and S. Mafe, "Electrochemical impedance spectroscopy of membranes with nanofluidic conical pores," J. Colloid Interface Sci. **655**, 876 (2024).
[53]J. Bisquert and A. Guerrero, "Chemical inductor," J. Am. Chem. Soc. **144**, 5996 (2022).
[54]J. Bisquert, M. Sanchez-Mateu, A. Bou, C. S. Law, and A. Santos, "Synaptic response of fluidic nanopores: The connection of potentiation with hysteresis," ChemPhysChem **25**, e202400265 (2024).
[55]T. Emmerich, Y. Teng, N. Ronceray, E. Lopriore, R. Chiesa, A. Chernev, V. Artemov, M. Di Ventra, A. Kis, and A. Radenovic, "Nanofluidic logic with mechano–ionic memristive switches," Nat. Electron. **7**, 271 (2024).
[56]S. L. Jackman and W. G. Regehr, "The mechanisms and functions of synaptic facilitation," Neuron **94**, 447 (2017).
[57]A. J. Hopper, H. Beswick-Jones, and A. M. Brown, "A color-coded graphical guide to the Hodgkin and Huxley papers," Adv. Physiol. Educ. **46**, 580 (2022).
[58]S. Menzel, S. Tappertzhofen, R. Waser, and I. Valov, "Switching kinetics of electrochemical metallization memory cells," Phys. Chem. Chem. Phys. **15**, 6945 (2013).
[59]I. Vourkas and G. C. Sirakoulis, "Emerging memristor-based logic circuit design approaches: A review," IEEE Circuits Syst. Mag. **16**, 15 (2016).
[60]P. Ramirez, V. Gómez, J. Cervera, S. Mafe, and J. Bisquert, "Synaptical tunability of multipore nanofluidic memristors," J. Phys. Chem. Lett. **14**, 10930 (2023).
[61]Y. Ling, L. Yu, Z. Guo, F. Bian, Y. Wang, X. Wang, Y. Hou, and X. Hou, "Single-pore nanofluidic logic memristor with reconfigurable synaptic functions and designable combinations," J. Am. Chem. Soc. **146**, 14558 (2024).
[62]B. Xie, T. Xiong, W. Li, T. Gao, J. Zong, Y. Liu, and P. Yu, "Perspective on nanofluidic memristors: From mechanism to application," Chem. Asian J. **17**, e202200682 (2022).
[63]D. Wang, J. Liu, M. Kvetny, Y. Li, W. Brown, and G. Wang, "Physical origin of dynamic ion transport features through single conical nanopores at different bias frequencies," Chem. Sci. **5**, 1827 (2014).
[64]Y. Bu, Z. Ahmed, and L. Yobas, "A nanofluidic memristor based on ion concentration polarization," Analyst **144**, 7168 (2019).
[65]W. Wang, Y. Liang, Y. Ma, D. Shi, and Y. Xie, "Memristive characteristics in an asymmetrically charged nanochannel," J. Phys. Chem. Lett. **15**, 6852 (2024).
[66]R. Yang, S. Kamila, D. Baram, and G. Wang, "Redox polymer-regulated hysteresis in ion current rectification through AAO membranes and single nanopipettes," Meet. Abstr. **MA2023-01**, 2575 (2023).
[67]C. Y. Lim, A. E. Lim, and Y. C. Lam, "Ionic origin of electro-osmotic flow hysteresis," Sci. Rep. **6**, 22329 (2016).
[68]N. Laohakunakorn and U. F. Keyser, "Electroosmotic flow rectification in conical nanopores," Nanotechnology **26**, 275202 (2015).
[69]W. Brown, M. Kvetny, R. Yang, and G. Wang, "Higher ion selectivity with lower energy usage promoted by electro-osmotic flow in the transport through conical nanopores," J. Phys. Chem. C **125**, 3269 (2021).
[70]W. Brown, Y. Li, R. Yang, D. Wang, M. Kvetny, H. Zheng, and G. Wang, "Deconvolution of electroosmotic flow in hysteresis ion transport through single asymmetric nanopipettes," Chem. Sci. **11**, 5950 (2020).
[71]D. Wang and G. Wang, "Dynamics of ion transport and electric double layer in single conical nanopores," J. Electroanal. Chem. **779**, 39 (2016).
[72]K. Chen, M. Tsutsui, F. Zhuge, Y. Zhou, Y. Fu, Y. He, and X. Miao, "Nanochannel-based interfacial memristor: Electrokinetic analysis of the frequency characteristics," Adv. Electron. Mater. **7**, 2000848 (2021).
[73]R. M. Adar, T. Markovich, and D. Andelman, "Bjerrum pairs in ionic solutions: A Poisson-Boltzmann approach," J. Chem. Phys. **146**, 194904 (2017).
[74]P. Robin, T. Emmerich, A. Ismail, A. Niguès, Y. You, G. H. Nam, A. Keerthi, A. Siria, A. K. Geim, B. Radha *et al.*, "Long-term memory and synapse-like dynamics in two-dimensional nanofluidic channels," Science **379**, 161 (2023).
[75]D. Shi, W. Wang, Y. Liang, L. Duan, G. Du, and Y. Xie, "Ultralow energy consumption angstrom-fluidic memristor," Nano Lett. **23**, 11662 (2023).
[76]Q. Sheng, Y. Xie, J. Li, X. Wang, and J. Xue, "Transporting an ionic-liquid/water mixture in a conical nanochannel: A nanofluidic memristor," Chem. Commun. **53**, 6125 (2017).
[77]M. Y. Chougale, M. U. Khan, J. Kim, R. A. Shaukat, Q. M. Saqib, S. R. Patil, T. D. Dongale, A. Bermak, B. Mohammad, and J. Bae, "Bioinspired soft multistate resistive memory device based on silk fibroin gel for neuromorphic computing," Adv. Eng. Mater. **24**, 2200314 (2022).
[78]T. T. Guo, J. B. Chen, C. Y. Yang, P. Zhang, S. J. Jia, Y. Li, J. T. Chen, Y. Zhao, J. Wang, and X. Q. Zhang, "Artificial neural synapses based on microfluidic memristors prepared by capillary tubes and ionic liquid," J. Phys. Chem. Lett. **15**, 2542 (2024).
[79]J. B. Chen, T. T. Guo, C. Y. Yang, J. W. Xu, L. Y. Gao, S. J. Jia, P. Zhang, J. T. Chen, Y. Zhao, J. Wang *et al.*, "Neuromorphic functions with a polyelectrolyte-confined fluidic memristor," J. Phys. Chem. C **127**, 3307 (2023).
[80]Z. Zhang, B. Sabbagh, Y. Chen, and G. Yossifon, "Geometrically scalable iontronic memristors: Employing bipolar polyelectrolyte gels for neuromorphic systems," ACS Nano **18**, 15025 (2024).
[81]D. Kim and J. S. Lee, "Emulating the signal transmission in a neural system using polymer membranes," ACS Appl. Mater. Interfaces **14**, 42308 (2022).
[82]S. H. Han, S. I. Kim, M. A. Oh, and T. D. Chung, "Iontronic analog of synaptic plasticity: Hydrogel-based ionic diode with chemical precipitation and dissolution," Proc. Natl. Acad. Sci. U. S. A. **120**, e2211442120 (2023).
[83]X. Zhou, Y. Zong, Y. Wang, M. Sun, D. Shi, W. Wang, G. Du, and Y. Xie, "Nanofluidic memristor based on the elastic deformation of nanopores with nanoparticle adsorption," Natl. Sci. Rev. **11**, nwad216 (2024).
[84]Y. Niu, Y. Ma, and Y. Xie, "Soft memristor at a microbubble interface," Nano Lett. **24**, 10475–10481 (2024).
[85]Y. Ma, Y. Niu, R. Pei, W. Wang, B. Wei, and Y. Xie, "Reconfigurable neuromorphic computing by a microdroplet," Cell Rep. Phys. Sci. **5**, 102202 (2024).
[86]Y. T. Xu, S. Y. Yu, Z. Li, B. H. Kou, J. X. Pang, W. W. Zhao, H. Y. Chen, and J. J. Xu, "A nanofluidic spiking synapse," Proc. Natl. Acad. Sci. U. S. A. **121**, e2403143121 (2024).
[87]P. Ramirez, S. Portillo, J. Cervera, S. Nasir, M. Ali, W. Ensinger, and S. Mafe, "Neuromorphic responses of nanofluidic memristors in symmetric and asymmetric ionic solutions," J. Chem. Phys. **160**, 0447001 (2024).
[88]P. Ramirez, J. Cervera, S. Nasir, M. Ali, W. Ensinger, and S. Mafe, "Memristive switching of nanofluidic diodes by ionic concentration gradients," Colloids Surf. A: Physicochem. Eng. Asp. **698**, 134525 (2024).
[89]S. Portillo, J. A. Manzanares, P. Ramirez, J. Bisquert, S. Mafe, and J. Cervera, "pH-dependent effects in nanofluidic memristors," J. Phys. Chem. Lett. **15**, 7793 (2024).
[90]P. Ramirez, S. Portillo, J. Cervera, J. Bisquert, and S. Mafe, "Memristive arrangements of nanofluidic pores," Phys. Rev. E **109**, 044803 (2024).
[91]J. Cao, X. Zhang, H. Cheng, J. Qiu, X. Liu, M. Wang, and Q. Liu, "Emerging dynamic memristors for neuromorphic reservoir computing," Nanoscale **14**, 289 (2022).
[92]A. Noy, Z. Li, and S. B. Darling, "Fluid learning: Mimicking brain computing with neuromorphic nanofluidic devices," Nano Today **53**, 102043 (2023).
[93]Y. He, L. Zhu, Y. Zhu, C. Chen, S. Jiang, R. Liu, Y. Shi, and Q. Wan, "Recent progress on emerging transistor-based neuromorphic devices," Adv. Intell. Syst. **3**, 2000210 (2021).
[94]F. J. Sigworth, "Life's transistors," Nature **423**, 21 (2003).
[95]T. Mei, W. Liu, G. Xu, Y. Chen, M. Wu, L. Wang, and K. Xiao, "Ionic transistors," ACS Nano **18**, 4624 (2024).
[96]S. Prakash and A. T. Conlisk, "Field effect nanofluidics," Lab Chip **16**, 3855 (2016).
[97]R. B. Schoch, J. Han, and P. Renaud, "Transport phenomena in nanofluidics," Rev. Mod. Phys. **80**, 839 (2008).
[98]H. Daiguji, "Ion transport in nanofluidic channels," Chem. Soc. Rev. **39**, 901 (2010).
[99]R. Karnik, R. Fan, M. Yue, D. Li, P. Yang, and A. Majumdar, "Electrostatic control of ions and molecules in nanofluidic transistors," Nano Lett. **5**, 943 (2005).

[100]G. Laucirica, Y. Toum-Terrones, V. M. Cayón, M. E. Toimil-Molares, O. Azzaroni, and W. A. Marmisollé, "Advances in nanofluidic field-effect transistors: External voltage-controlled solid-state nanochannels for stimulus-responsive ion transport and beyond," Phys. Chem. Chem. Phys. **26**, 10471 (2024).
[101]S. Sagar, K. Udaya Mohanan, S. Cho, L. A. Majewski, and B. C. Das, "Emulation of synaptic functions with low voltage organic memtransistor for hardware oriented neuromorphic computing," Sci. Rep. **12**, 3808 (2022).
[102]K. Xiao, L. Wen, and L. Jiang, "Biomimetic solid-state nanochannels: From fundamental research to practical applications," Small **12**, 2810–2831 (2016).
[103]X. Hou, W. Guo, and L. Jiang, "Biomimetic smart nanopores and nanochannels," Chem. Soc. Rev. **40**, 2385 (2011).
[104]H. Zhang, Y. Tian, and L. Jiang, "Fundamental studies and practical applications of bio-inspired smart solid-state nanopores and nanochannels," Nano Today **11**, 61 (2016).
[105]Z. S. Siwy and S. Howorka, "Engineered voltage-responsive nanopores," Chem. Soc. Rev. **39**, 1115 (2010).
[106]P. Liu, X. Y. Kong, L. Jiang, and L. Wen, "Ion transport in nanofluidics under external fields," Chem. Soc. Rev. **53**, 2972 (2024).
[107]H. Zhang, Y. Tian, and L. Jiang, "From symmetric to asymmetric design of bio-inspired smart single nanochannels," Chem. Commun. **49**, 10048 (2013).
[108]W. Guan, R. Fan, and M. A. Reed, "Field-effect reconfigurable nanofluidic ionic diodes," Nat. Commun. **2**, 506 (2011).
[109]S. W. Nam, M. J. Rooks, K. B. Kim, and S. M. Rossnagel, "Ionic field effect transistors with sub-10 nm multiple nanopores," Nano Lett. **9**, 2044 (2009).
[110]M. Nishizawa, V. P. Menon, and C. R. Martin, "Metal nanotubule membranes with electrochemically switchable ion-transport selectivity," Science **268**, 700 (1995).
[111]E. B. Kalman, O. Sudre, I. Vlassiouk, and Z. S. Siwy, "Control of ionic transport through gated single conical nanopores," Anal. Bioanal. Chem. **394**, 413 (2009).
[112]M. Fuest, C. Boone, K. K. Rangharajan, A. T. Conlisk, and S. Prakash, "A three-state nanofluidic field effect switch," Nano Lett. **15**, 2365 (2015).
[113]M. Fuest, K. K. Rangharajan, C. Boone, A. T. Conlisk, and S. Prakash, "Cation dependent surface charge regulation in gated nanofluidic devices," Anal. Chem. **89**, 1593 (2017).
[114]R. Fan, M. Yue, R. Karnik, A. Majumdar, and P. Yang, "Polarity switching and transient responses in single nanotube nanofluidic transistors," Phys. Rev. Lett. **95**, 086607 (2005).
[115]R. Karnik, K. Castelino, and A. Majumdar, "Field-effect control of protein transport in a nanofluidic transistor circuit," Appl. Phys. Lett. **88**, 123114 (2006).
[116]H. Hong, X. Lei, J. Wei, Y. Zhang, Y. Zhang, J. Sun, G. Zhang, P. M. Sarro, and Z. Liu, "Rectification in ionic field effect transistors based on single crystal silicon nanopore," Adv. Electron. Mater. **10**, 2300782 (2024).
[117]N. Hu, Y. Ai, and S. Qian, "Field effect control of electrokinetic transport in micro/nanofluidics," Sens. Actuators B: Chem. **161**, 1150 (2012).
[118]G. Pérez-Mitta, W. A. Marmisolleé, C. Trautmann, M. E. Toimil-Molares, and O. Azzaroni, "Nanofluidic diodes with dynamic rectification properties stemming from reversible electrochemical conversions in conducting polymers," J. Am. Chem. Soc. **137**, 15382 (2015).
[119]G. Laucirica, W. A. Marmisolleé, M. E. Toimil-Molares, C. Trautmann, and O. Azzaroni, "Redox-driven reversible gating of solid-state nanochannels," ACS Appl. Mater. Interfaces **11**, 30001 (2019).
[120]Q. Zhang, Z. Zhang, H. Zhou, Z. Xie, L. Wen, Z. Liu, J. Zhai, and X. Diao, "Redox switch of ionic transport in conductive polypyrrole-engineered unipolar nanofluidic diodes," Nano Res. **10**, 3715 (2017).
[121]G. Laucirica, V. M. Cayón, Y. T. Terrones, M. L. Cortez, M. E. Toimil-Molares, C. Trautmann, W. A. Marmisollé, and O. Azzaroni, "Electrochemically addressable nanofluidic devices based on PET nanochannels modified with electropolymerized poly-o-aminophenol films," Nanoscale **12**, 6002 (2020).
[122]G. Laucirica, Y. T. Terrones, M. F. Wagner, V. M. Cayón, M. L. Cortez, M. E. Toimil-Molares, C. Trautmann, W. Marmisollé, and O. Azzaroni, "Electrochemically addressed FET-like nanofluidic channels with dynamic ion-transport regimes," Nanoscale **15**, 1782 (2023).
[123]R. Wu, J. Hao, Y. Cui, J. Zhou, D. Zhao, S. Zhang, J. Wang, Y. Zhou, and L. Jiang, "Multi-control of ion transport in a field-effect iontronic device based on sandwich-structured nanochannels," Adv. Funct. Mater. **33**, 2208095 (2023).
[124]G. Pérez-Mitta, W. A. Marmisollé, C. Trautmann, M. E. Toimil-Molares, and O. Azzaroni, "An all-plastic field-effect nanofluidic diode gated by a conducting polymer layer," Adv. Mater. **29**, 1700972 (2017).
[125]Y. L. Hu, Y. Hua, Z. Q. Pan, J. H. Qian, X. Y. Yu, N. Bao, X. L. Huo, Z. Q. Wu, and X. H. Xia, "PNP nanofluidic transistor with actively tunable current response and ionic signal amplification," Nano Lett. **22**, 3678 (2022).
[126]W. Xin, H. Ling, Y. Cui, Y. Qian, X. Y. Kong, L. Jiang, and L. Wen, "Tunable ion transport in two-dimensional nanofluidic channels," J. Phys. Chem. Lett. **14**, 627 (2023).
[127]Y. Wang, H. Zhang, Y. Kang, Y. Zhu, G. P. Simon, and H. Wang, "Voltage-gated ion transport in two-dimensional sub-1 nm nanofluidic channels," ACS Nano **13**, 11793 (2019).
[128]C. Cheng, G. Jiang, G. P. Simon, J. Z. Liu, and D. Li, "Low-voltage electrostatic modulation of ion diffusion through layered graphene-based nanoporous membranes," Nat. Nanotechnol. **13**, 685 (2018).
[129]Y. Xue, Y. Xia, S. Yang, Y. Alsaid, K. Y. Fong, Y. Wang, and X. Zhang, "Atomic-scale ion transistor with ultrahigh diffusivity," Science **372**, 501 (2021).
[130]S. H. Lee, H. Lee, T. Jin, S. Park, B. J. Yoon, G. Y. Sung, K. B. Kim, and S. J. Kim, "Sub-10 nm transparent all-around-gated ambipolar ionic field effect transistor," Nanoscale **7**, 936–946 (2015).
[131]Q. Zhang, J. Kang, Z. Xie, X. Diao, Z. Liu, and J. Zhai, "Highly efficient gating of electrically actuated nanochannels for pulsatile drug delivery stemming from a reversible wettability switch," Adv. Mater. **30**, 1703323 (2018).
[132]W. Noh, S. Pak, G. Choi, S. Yang, and S. Yang, "Transient potassium channels: Therapeutic targets for brain disorders," Front. Cell. Neurosci. **13**, 265 (2019).
[133]K. Wu, K. Xiao, L. Chen, R. Zhou, B. Niu, Y. Zhang, and L. Wen, "Biomimetic voltage-gated ultrasensitive potassium-activated nanofluidic based on a solid-state nanochannel," Langmuir **33**, 8463 (2017).
[134]W. Liu, T. Mei, Z. Cao, C. Li, Y. Wu, L. Wang, G. Xu, Y. Chen, Y. Zhou, S. Wang, and Y. Xue, "Bioinspired carbon nanotube–based nanofluidic ionic transistor with ultrahigh switching capabilities for logic circuits," Sci. Adv. **10**, eadj7867 (2024).
[135]T. Mei, W. Liu, F. Sun, Y. Chen, G. Xu, Z. Huang, Y. Jiang, S. Wang, L. Chen, J. Liu, and F. Fan, "Bio-inspired two-dimensional nanofluidic ionic transistor for neuromorphic signal processing," Angew. Chem. Int. Ed. Engl. **63**, e202401477 (2024).
[136]X. Xu, H. Zhang, L. Shao, R. Ma, M. Guo, Y. Liu, and Y. Zhao, "An aqueous electrolyte gated artificial synapse with synaptic plasticity selectively mediated by biomolecules," Angew. Chem. Int. Ed. **62**, e202302723 (2023).
[137]B. Sabbagh, N. E. Fraiman, A. Fish, and G. Yossifon, "Designing with iontronic logic gates–from a single polyelectrolyte diode to an integrated ionic circuit," ACS Appl. Mater. Interfaces **15**, 23361 (2023).
[138]B. Sabbagh, Z. Zhang, and G. Yossifon, "Logic gating of low-abundance molecules using polyelectrolyte-based diodes," Faraday Discuss. **246**, 141 (2023).
[139]A. L. Hodgkin and A. F. Huxley, "A quantitative description of membrane current and its application to conduction and excitation in nerve," J. Physiol. **117**, 500 (1952).
[140]H. R. Wilson, *Spikes, Decisions, and Actions: The Dynamical Foundations of Neuroscience* (Oxford University Press, Oxford, 1999).
[141]S. H. Strogatz, *Nonlinear Dynamics and Chaos*, 2nd ed. (CRC Press, Florida, 2019).
[142]E. M. Izhikevich, *Dynamical Systems in Neuroscience* (MIT Press, Massachusetts, 2007).
[143]M. T. Koper, "Stability study and categorization of electrochemical oscillators by impedance spectroscopy," J. Electroanal. Chem. **409**, 175 (1996).
[144]J. Bisquert, "Iontronic nanopore model for artificial neurons: The requisites of spiking," J. Phys. Chem. Lett. **14**, 9027 (2023).
[145]A. Cordero, J. R. Torregrosa, and J. Bisquert, "Bifurcation and oscillations in fluidic nanopores: A model neuron for liquid neuromorphic networks," Phys. Rev. Res. **7**, 013282 (2025).
[146]M. T. Koper, "Non-linear phenomena in electrochemical systems," Faraday Trans. **94**, 1369 (1998).